

Ring Current Dynamics

Vania K. Jordanova

Los Alamos National Laboratory, NM, USA

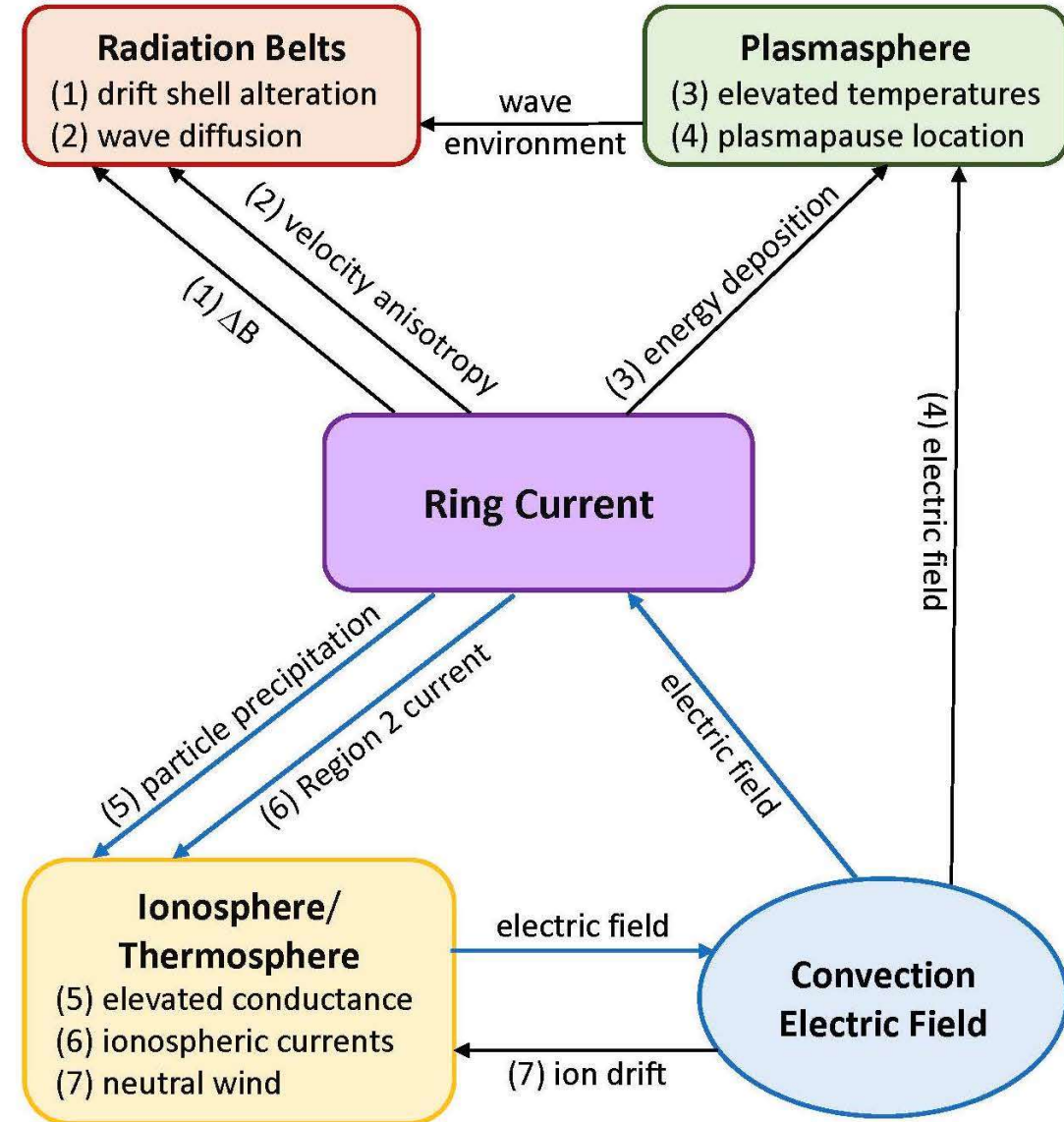
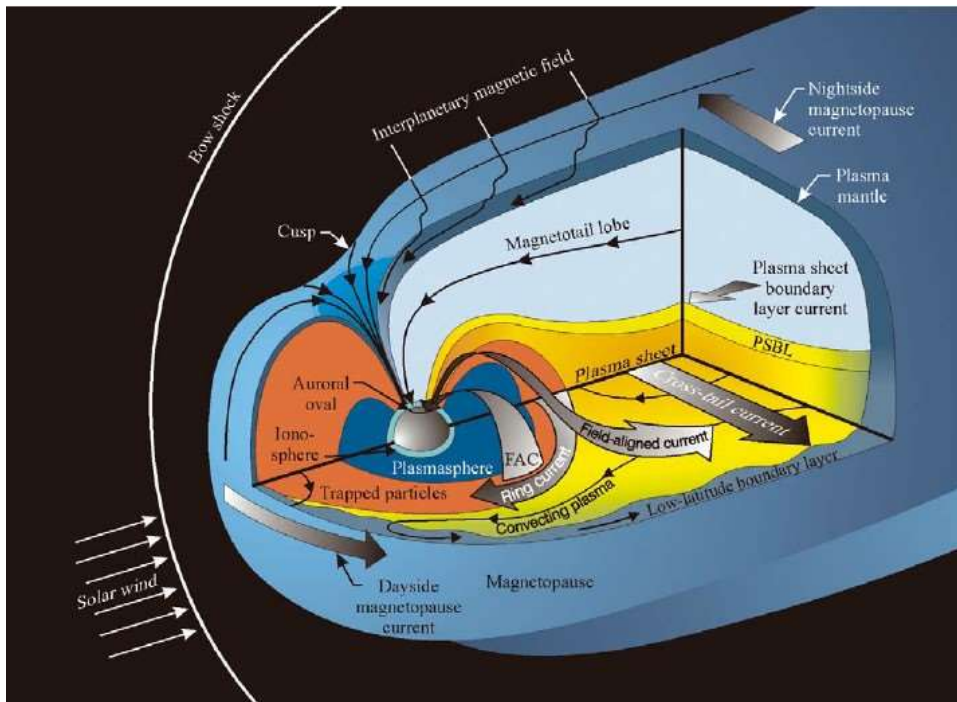
(*vania@lanl.gov*)

Magnetosphere Online Seminar Series
21 September 2020

This presentation is being recorded



Inner Magnetosphere Cross-Regional Coupling



- Important processes that couple the ring current with other regions
- Ring current particles are lost through collisions with neutral and charged particles from the geocorona and plasmasphere
- The blue arrows highlight the electric coupling cycle connecting the ring current and the ionosphere

[Ring Current Investigations, Elsevier Book, 2020,
<https://doi.org/10.1016/C2017-0-03448-1>]



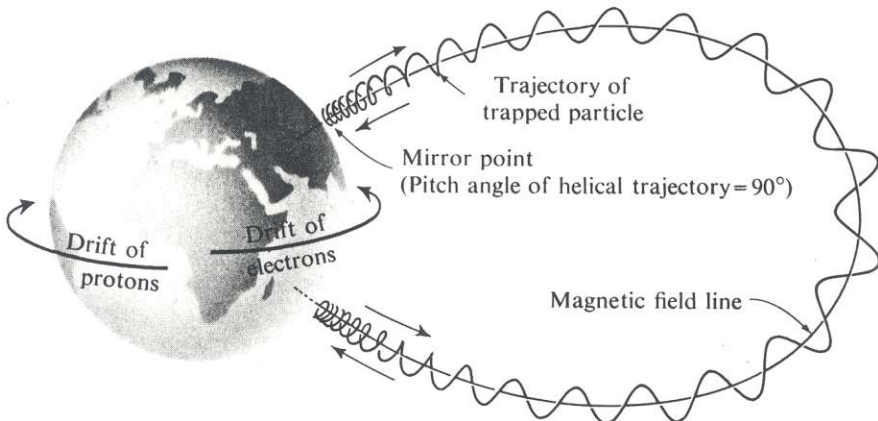
Theoretical Approaches for Studying Ring Current Dynamics

- **Single particle motion** - describes the motion of a particle under the influence of external electric and magnetic fields
 - trajectory tracing studies
 - mapping of distribution function
- **Magnetohydrodynamics (MHD) and Multi-Fluid theory** - the plasma is treated as conducting fluids with macroscopic variables, allow self-consistent coupling of the magnetosphere and ionosphere
- **Kinetic theory** - adopts a statistical approach and looks at the development of the distribution function for a system of particles

I. Transport in Electric and Magnetic Fields

This presentation is being recorded

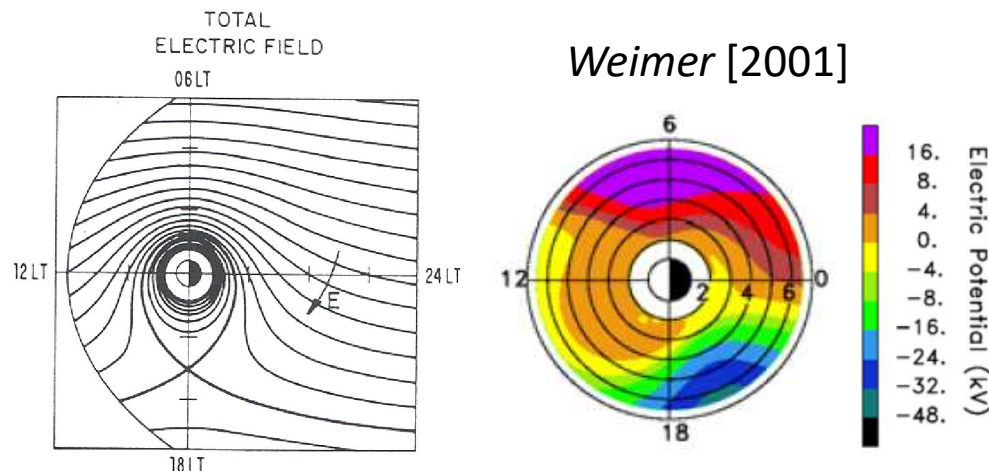
Large-Scale Transport in Realistic Fields



- The **Earth's magnetic field** is the sum of several contributions including the main **internal** (dipolar) field and the **external** source (magnetospheric) fields [e.g., *Tsyganenko, 1989, 2004*].

Gradient-Curvature velocity:

$$\vec{v}_{GC} = -\frac{m_s}{qB^4} \left(v_{II}^2 + \frac{v_\perp^2}{2} \right) \left(\nabla \frac{B^2}{2} \right) \times \vec{B}$$



[*Lyons and Williams, 1984*]

- Volland-Stern semi-empirical model **convection** potential:

$$U_{conv} = AR_o^\gamma \sin(\phi - \phi_o)$$

corotation potential:

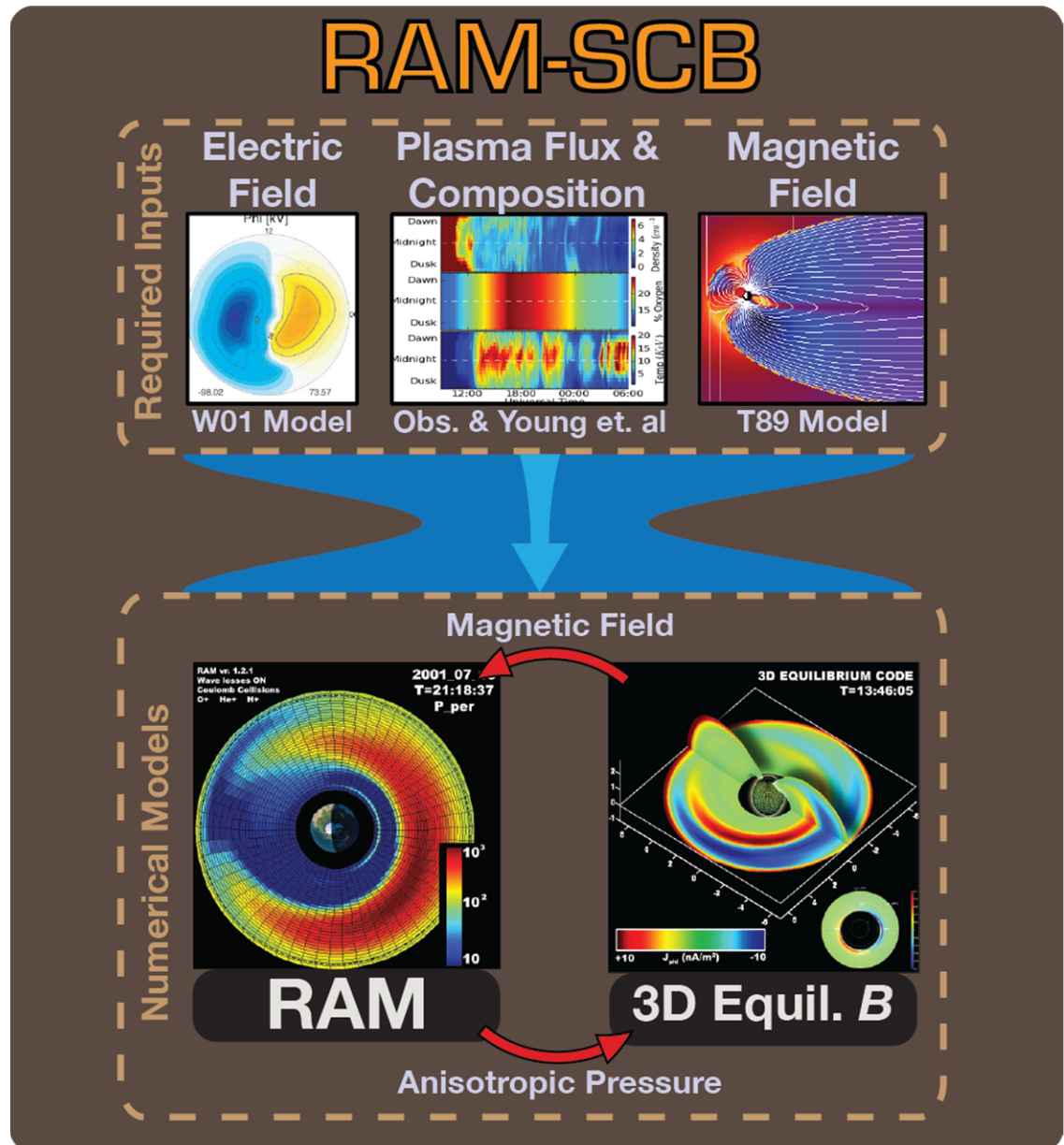
$$U_{cor} = -C/R_o$$

Drift velocity:

$$\vec{v}_{DE} = \frac{\vec{E} \times \vec{B}}{B^2}, \quad \vec{E} = -\nabla U$$

Ring current - Atmosphere interactions Model with Self-Consistent Magnetic field (RAM-SCB)

- » Ring current-atmosphere interactions model (RAM)
[Jordanova et al., 1994, 2010; 2016]
 - Kinetic equation for H⁺, O⁺, and He⁺ ions and electrons
 - Including all major loss processes
 - Convection and corotation E field
 - Updated to general B field
- » 3D equilibrium code
[Cheng, 1995; Zaharia et al., 2004; 2010; Engel et al., 2019]
 - Force-balanced equation
$$\mathbf{J} \times \mathbf{B} - \nabla \cdot \mathbf{P} = 0$$
 - Euler potentials (flux coordinates)
- » Boundary conditions at 6.5 or 9 R_E
[Tsyganenko and Mukai, 2003] as functions of incoming solar wind and IMF parameters; ion composition after [Mouikis et al., 2010]



RAM-SCB: Governing Equations

► Kinetic equation solved in RAM:

$$\frac{\partial Q_l}{\partial t} + \frac{1}{R_o^2} \frac{\partial}{\partial R_o} \left(R_o^2 \left\langle \frac{dR_o}{dt} \right\rangle Q_l \right) + \frac{\partial}{\partial \phi} \left(\left\langle \frac{d\phi}{dt} \right\rangle Q_l \right) + \frac{1}{\gamma p} \frac{\partial}{\partial E} \left(\gamma p \left\langle \frac{dE}{dt} \right\rangle Q_l \right) + \frac{1}{h\mu_o} \frac{\partial}{\partial \mu_o} \left(h\mu_o \left\langle \frac{d\mu_o}{dt} \right\rangle Q_l \right) = \left\langle \left(\frac{\partial Q_l}{\partial t} \right)_{loss} \right\rangle$$

where $Q_l = \frac{dN_l}{dV}$ and $dV = 8\pi m_o \gamma p R_o^2 \mu_o h(\mu_o) dR_o d\phi dE d\mu_o$

$$R_o = 2.0 - 6.5 R_E; \text{ all MLT}; \quad E = 100 \text{ eV} - 400 \text{ keV}; \quad \alpha_o = 0^\circ - 90^\circ; \quad \mu_o = \cos \alpha_o$$

► Bounce-averaging between mirror points:

$$\langle \chi \rangle = \frac{1}{S_B} \int_{s_m}^{s_m'} \chi \frac{ds}{\sqrt{1 - B(s)/B_m}}$$

$$h(\mu_o) = \frac{1}{2R_o} \int_{s_m}^{s_m'} \frac{ds}{\sqrt{1 - B(s)/B_m}}$$

► Self-consistently calculated 3D magnetic field in force balance with anisotropic plasma pressures from RAM:

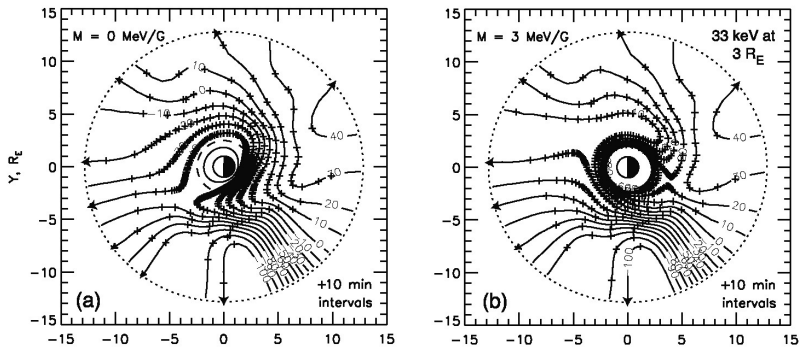
$$\nabla \cdot [(\nabla \alpha)^2 \nabla \beta - (\nabla \alpha \cdot \nabla \beta) \nabla \alpha] = - \frac{(\mathbf{B} \times \nabla \alpha)}{\sigma B^2} \cdot \left[\nabla P_\perp + (1 - \sigma) \nabla \left(\frac{B^2}{2} \right) \right]$$

$$\nabla \cdot [(\nabla \alpha \cdot \nabla \beta) \nabla \beta - (\nabla \beta)^2 \nabla \alpha] = - \frac{(\mathbf{B} \times \nabla \beta)}{\sigma B^2} \cdot \left[\nabla P_\perp + (1 - \sigma) \nabla \left(\frac{B^2}{2} \right) \right]$$

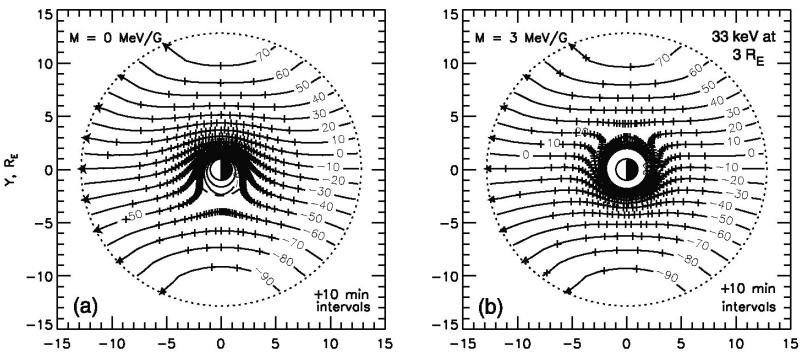
where $\mathbf{B} = \nabla \alpha \times \nabla \beta$, $\sigma = 1 + (P_\perp - P_{||})/B^2$ and α and β are the Euler potentials

Transport in High-Resolution Electric Field

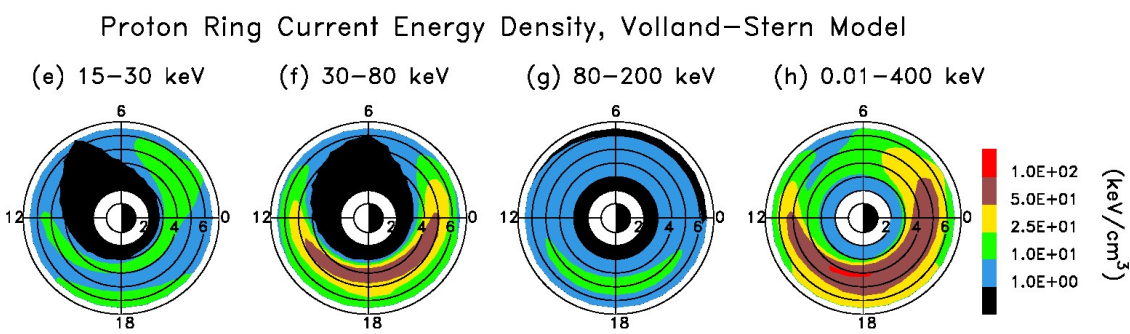
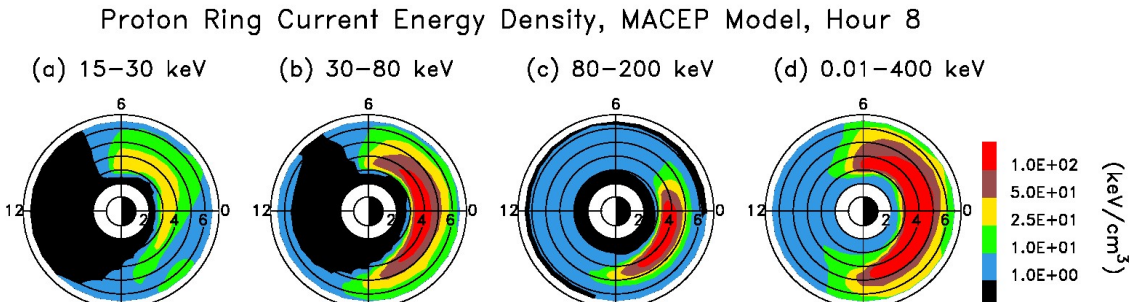
A) AMIE model



B) Simplified model

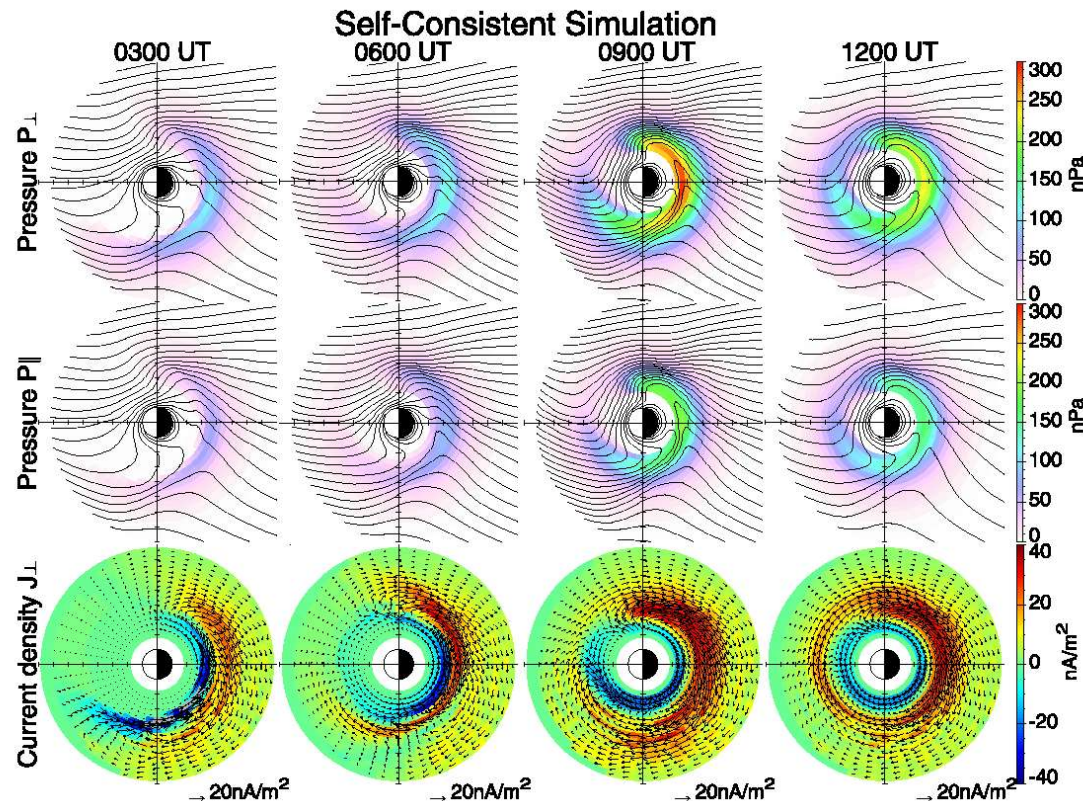


Equatorial quasi-steady drift paths of ions during the main phase of the 19 October 1998 storm in snapshots of two electric field models [Chen *et al.*, 2003]

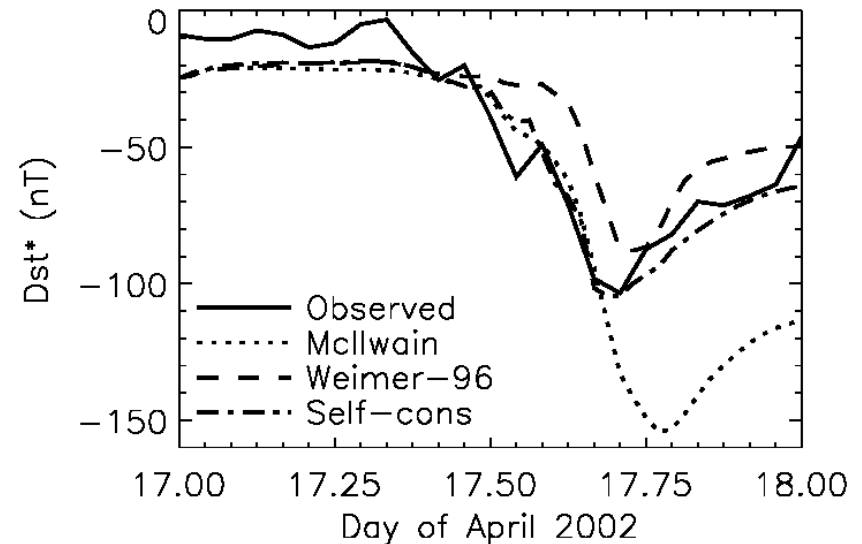


Proton ring current energy density during the main phase of the 10 January 1997 storm using two electric field models [Jordanova *et al.*, 2003]

Transport in Self-Consistent Electric Field

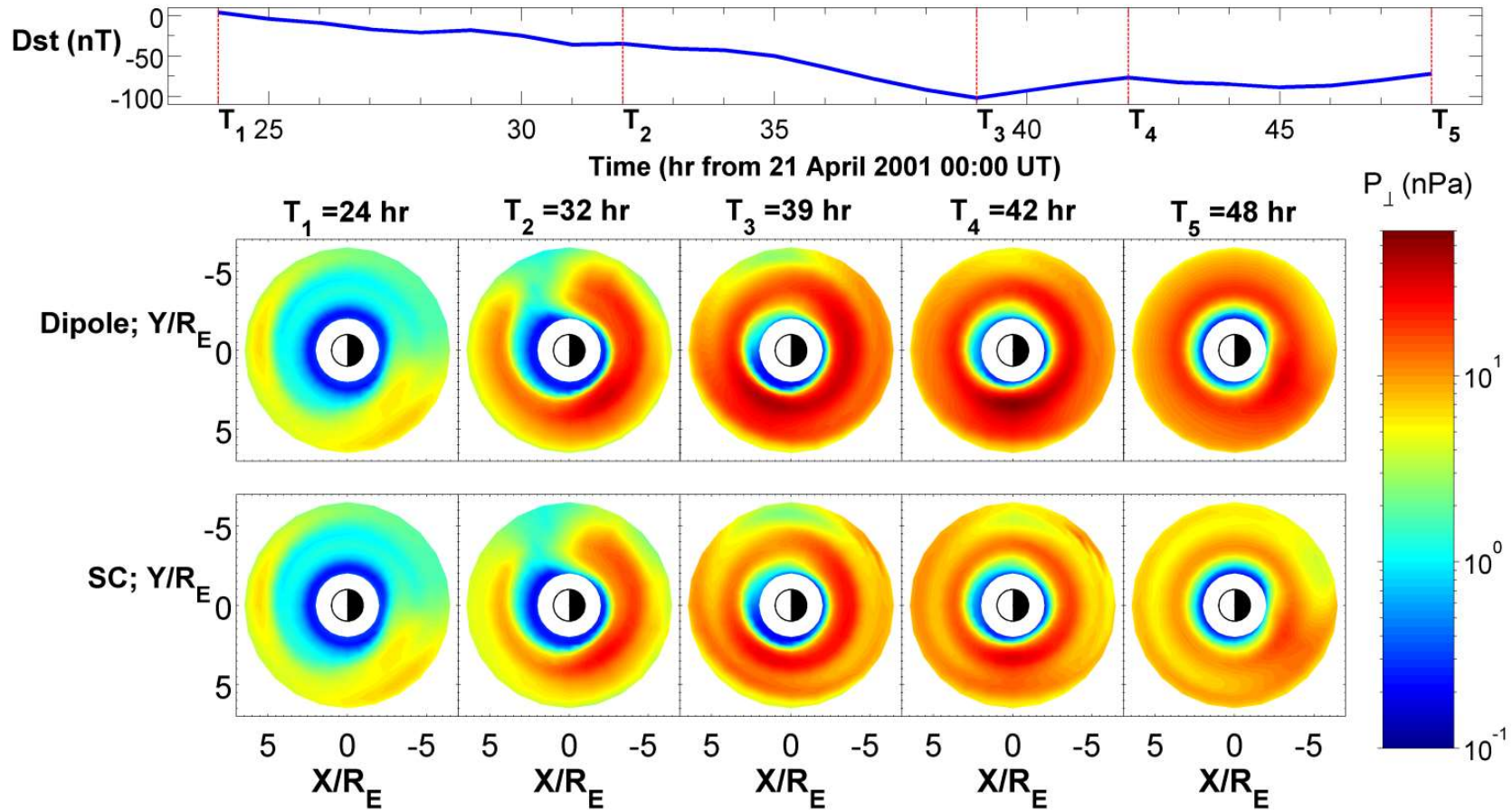


Ring current parameters during the 12 August 2000 storm [Ebihara *et al.*, 2004] using the CRCM, which couples the Fok *et al.* [2001] ring current model with the Rice Convection Model [Wolf *et al.*, 1982]



Dst^* from RAM using three electric field descriptions: modified McIlwain, Weimer 96 model, and a self-consistent Poisson equation solution [Liemohn *et al.*, 2004]

RAM-SCB: Effect of Magnetic Self-Consistency

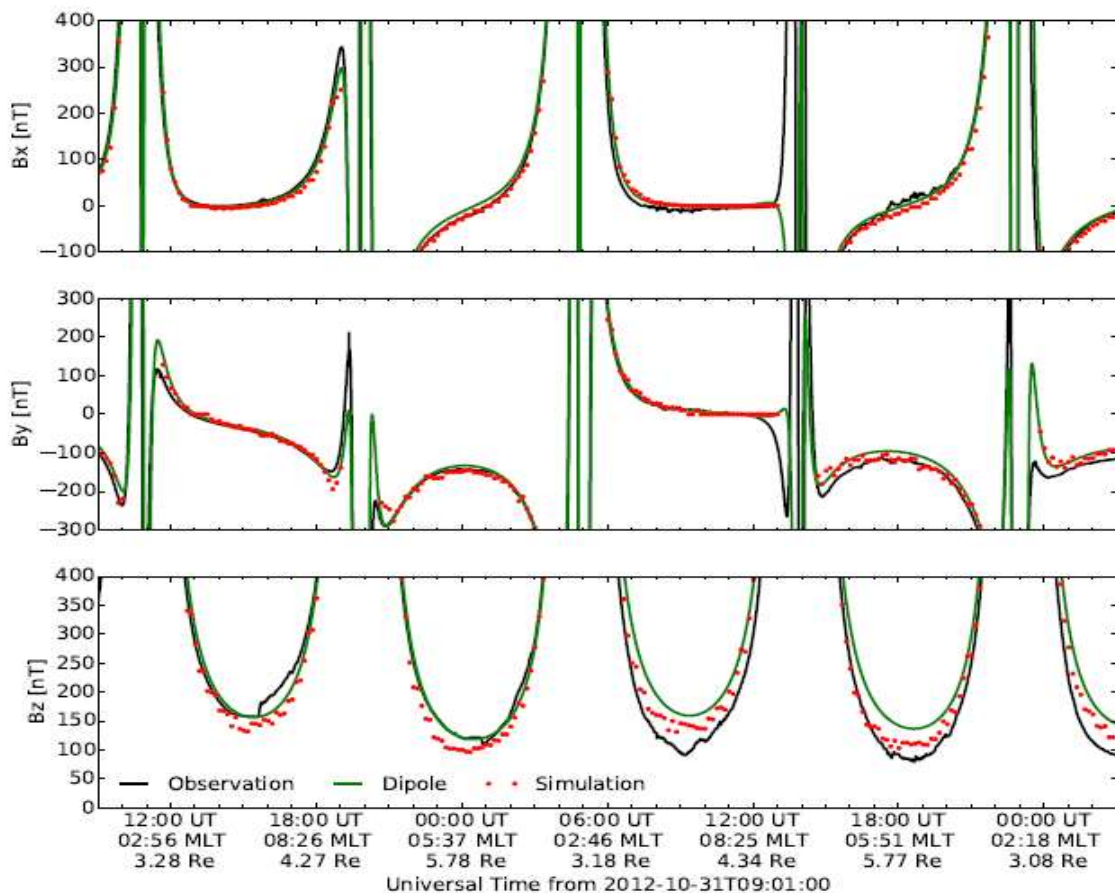


[Zaharia et al., 2006]

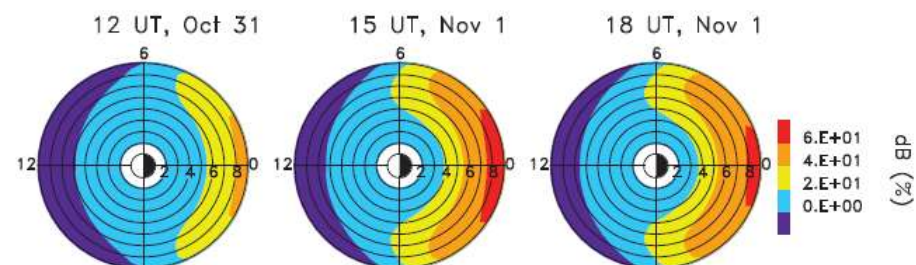
- Largest pressure at dusk-premidnight in storm main phase
- Self-consistent (SC) pressure is lower vs. RAM dipolar run (30 nPa max. vs. 60 nPa)
- Fine SC structure: local gradients, double peaks; larger pressure farther away

Comparisons with RBSP/EMFISIS Magnetometer Data

Along RBSP-B orbit



Relative difference between RAM-SCB magnetic field intensity and Earth's dipolar field

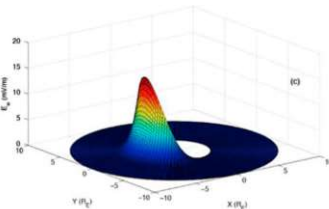


Depression larger than 60% at $L>8$ on the nightside during storm main phase

[Jordanova et al., 2014]

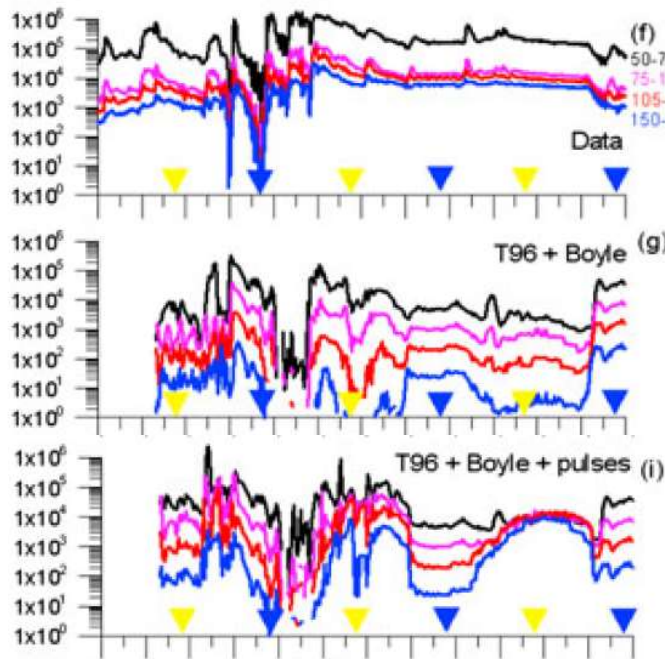
- Dipolar magnetic field at $L<4$; gets increased on the dayside due to the magnetopause current, and decreased on the nightside due to the ion pressure buildup
- RAM-SCB reproduces better the large-scale magnetic field components measured by EMFISIS magnetometer compared to a dipolar field

Role of Induced Electric Field



Including an earthward-propagating electromagnetic pulse

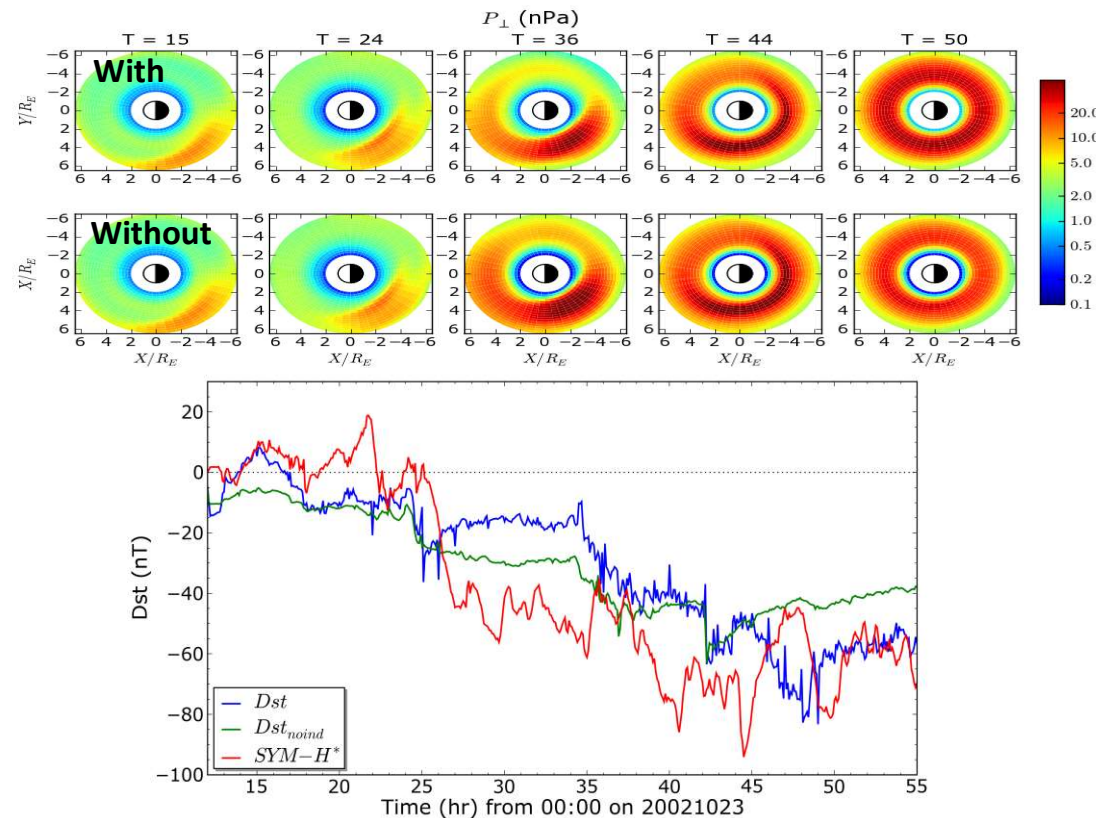
June 12-14, 2005 storm: Comparison with LANL01A electron flux data



Transport of low-E (50-250 keV) electrons with IMPTAM model [Ganushkina et al., 2013] from 10 Re to GEO shows **increase in the electron fluxes up to 2 orders of magnitude** when substorm-associated impulsive fields are taken into account

This presentation is being recorded

Calculating E-field induced by B-field changes in 3-D code SCB



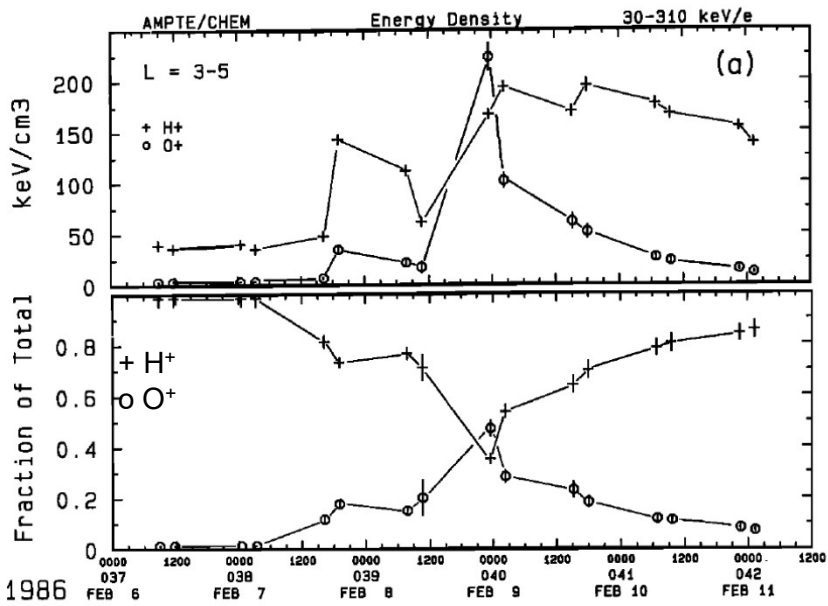
- E_{ind} slightly decreases ring current pressure in main phase but significantly increases ring current pressure in recovery phase
- Effect of induced E-field: weaker main phase ring current, but **stronger at peak (by ~ 50%) and during recovery phase** [Zaharia et al., 2008]

II. Ring Current Sources and Ion Composition

This presentation is being recorded



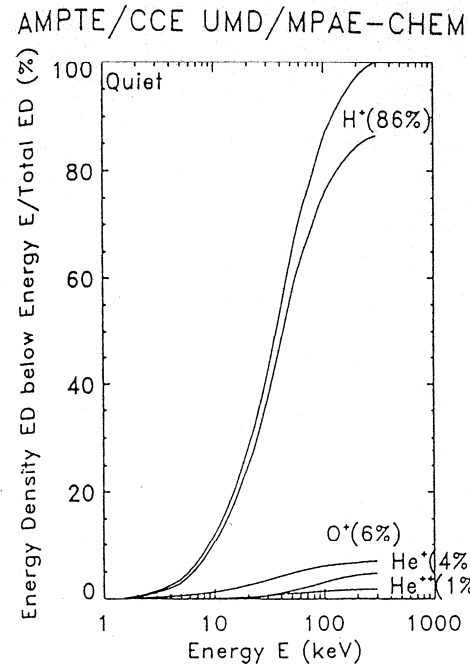
Ring Current Ion Composition



Energy density of ring current H⁺ and O⁺ during the major storm of Feb 9, 1986 with Dst=-312 nT after data from AMPTE CHEM at **L=3-5** [Hamilton *et al.*, 1988]

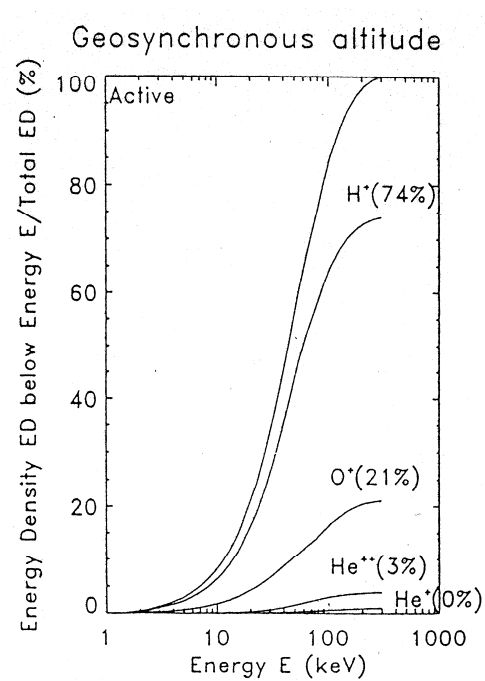
- The densities of both H⁺ and O⁺ increased during the storm but the relative **increase of O⁺** was much greater
- **Dominance of O⁺ density near minimum Dst**
- Statistics after [Gloeckler and Hamilton, 1987]:

 - moderate storms: 77% H⁺, **21% O⁺**
 - major storm: 36% H⁺, **47% O⁺**

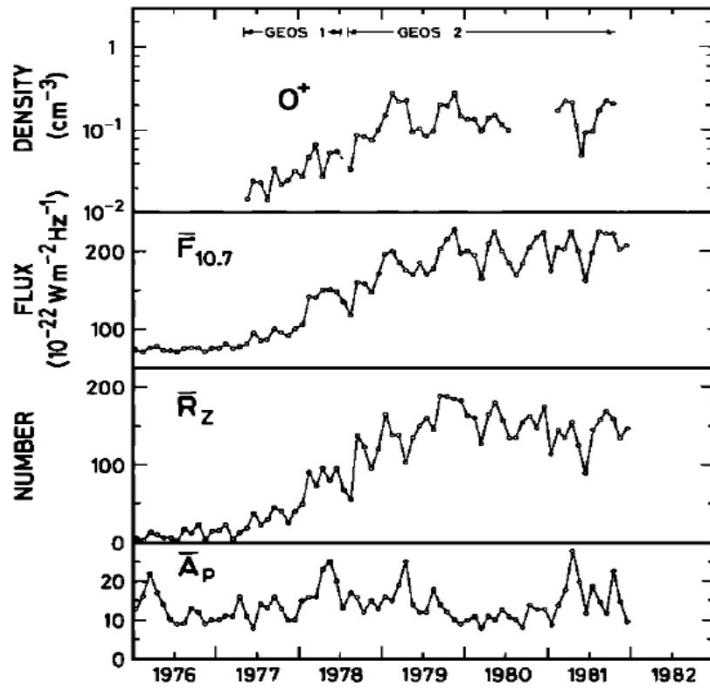


Ion energy density obtained from AMPTE/CHEM measurements averaged over 2.5 years [Daglis *et al.*, 1993]

- Ions in the energy range ~10-100 keV contribute most to the total energy density
- The dominant ring current ion species is H⁺ with O⁺ contributing mostly during active times



Plasma Sheet Source Populations

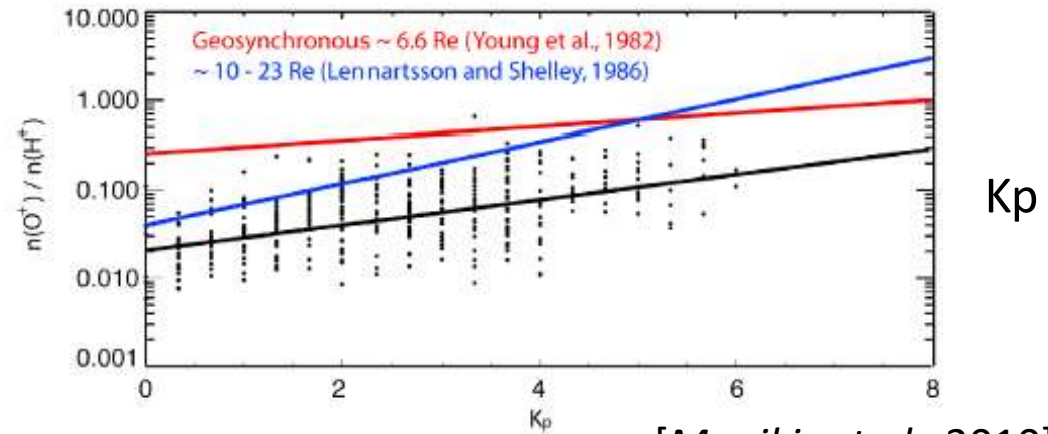
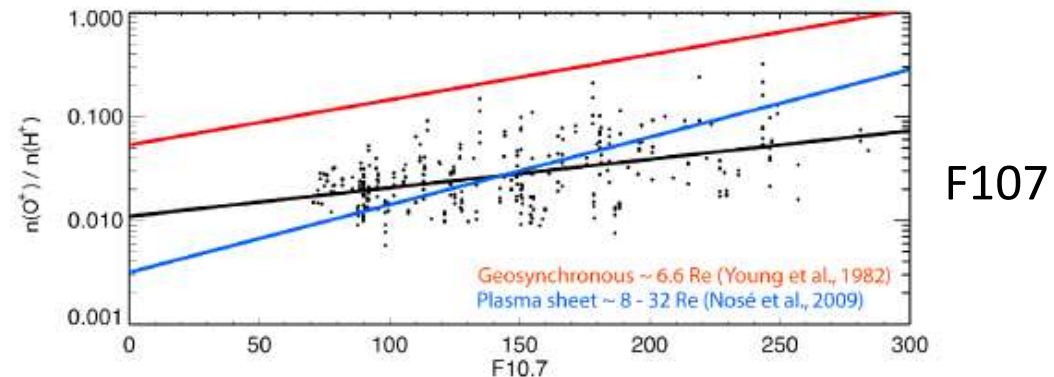


[Young et al., 1982]

- Data from GEOS satellites, $E=1\text{--}16$ keV, geostationary orbit
- Magnetospheric **O⁺ density increases systematically** by an order of magnitude during the rising of the **solar cycle**
- Notable increase of O⁺ density with **geomagnetic activity**

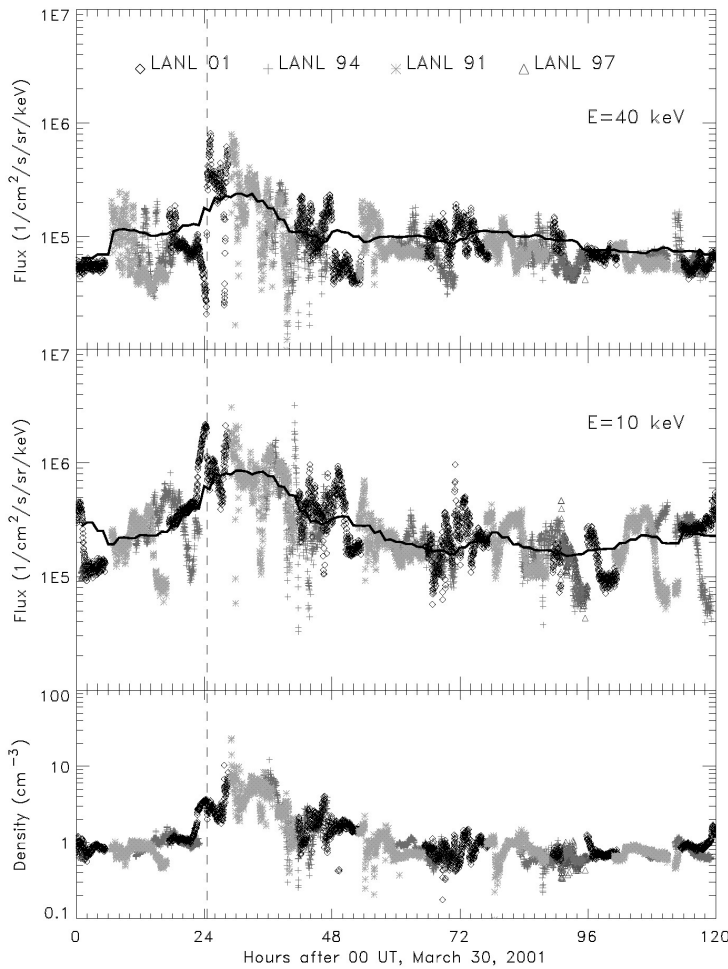
Data from Cluster satellites from 15 to 19 Re downtail from 2001 to 2005:

- O⁺ density depends strongly on solar EUV and geomagnetic activity
- Indication of additional entry of O⁺ inside of 15 Re
- Small MLT dependence, **H⁺ increase on flanks**

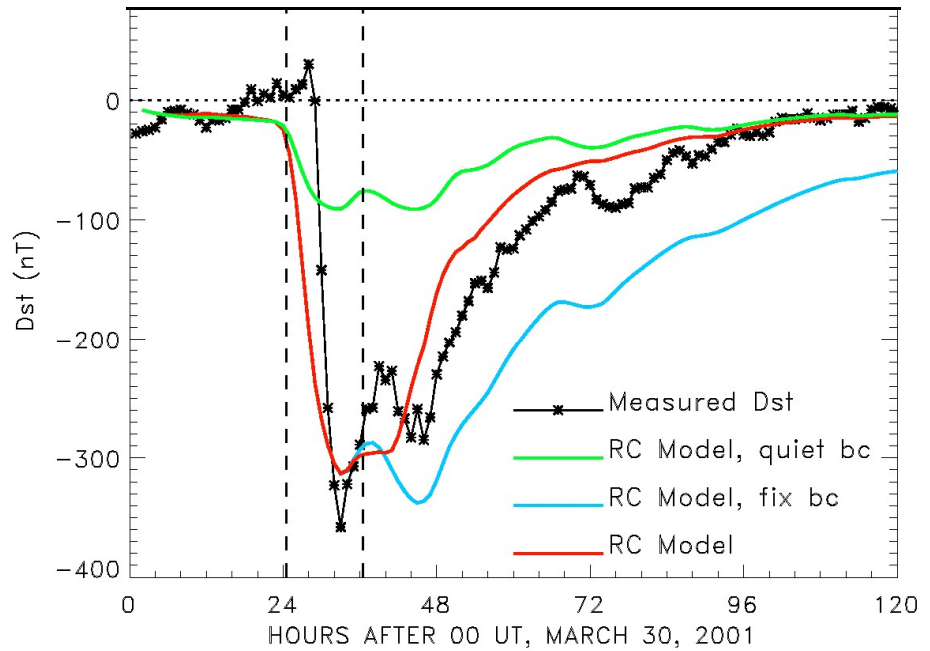


[Mouikis et al., 2010]

Effects of Time-Dependent Plasma Sheet Source Population



- Enhanced fluxes are observed in both energy channels of the MPA instrument for ~10 hours after the IP shock
- The magnitude of the ion fluxes gradually decreases after that



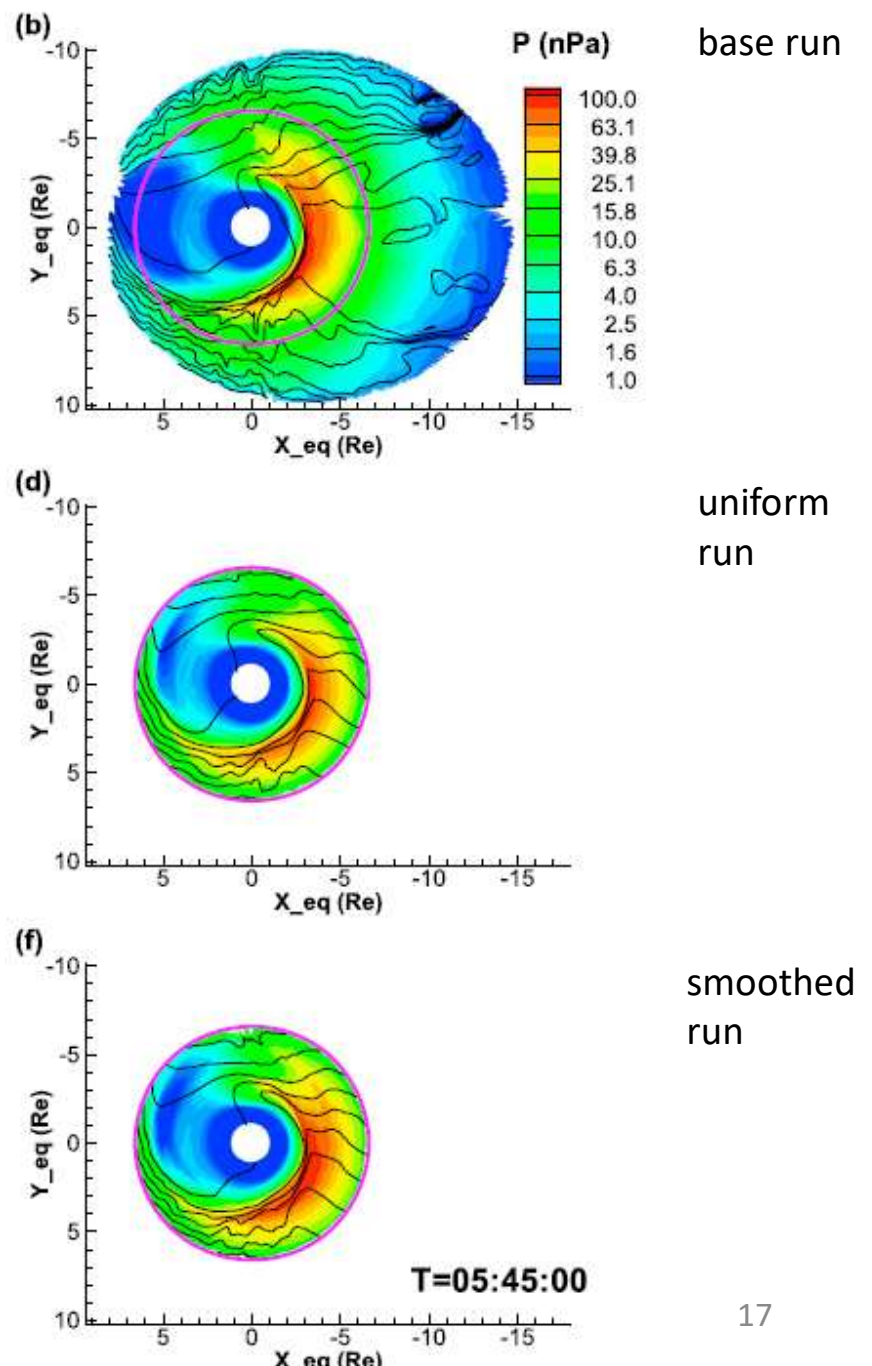
- Enhancement in the convection electric field alone is not sufficient to reproduce the Dst index
- The ring current (RC) increases significantly when the stormtime enhancement of plasma sheet density is considered
- The drop of plasma sheet density during early recovery phase is important for the fast RC decay

[Jordanova et al., 2003]

Particle Transport from the Plasma Sheet

- High-resolution simulations with the Rice Convection Model-Equilibrium of an idealized storm with random injection of BBFs/bubbles on the nightside
- **Without transient injections (no bubbles), plasma is not efficiently transported and accelerated from 15 Re to geosynchronous, so no significant ring current is formed**
- **The difference in plasma pressure between the three test runs is smaller than 10%, showing that buoyancy effects inside GEO have minor effect on ring current structure**

[Yang et al., 2015, 2016]



III. Ring Current Losses



This presentation is being recorded

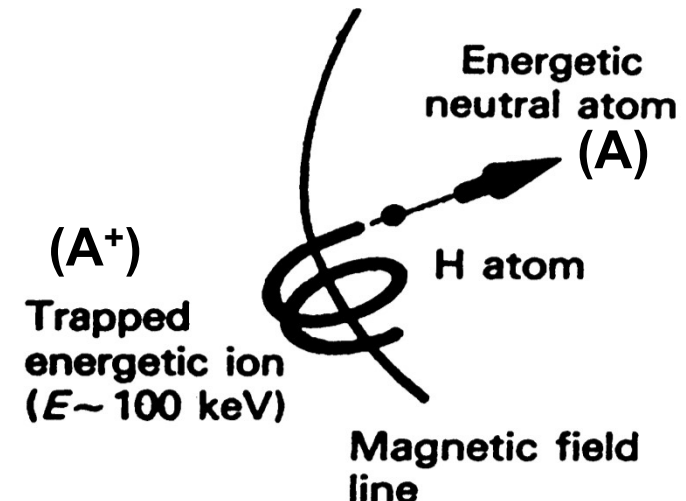
RAM-SCB: Ring Current Loss Processes

■ Charge exchange with Hydrogen from geocorona

$$\left\langle \left(\frac{dQ}{dt} \right)_{ce} \right\rangle = -\sigma_t \sqrt{\frac{2E}{m_t}} \langle n_H \rangle Q$$

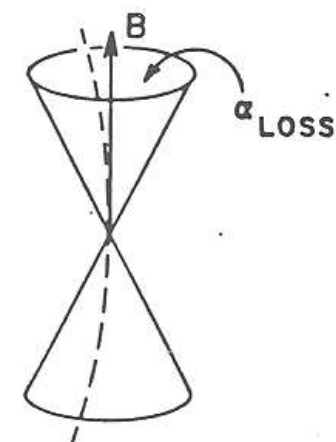
σ_t - cross section for charge exchange with H

$\langle n_H \rangle$ - bounce-averaged exospheric Hydrogen density

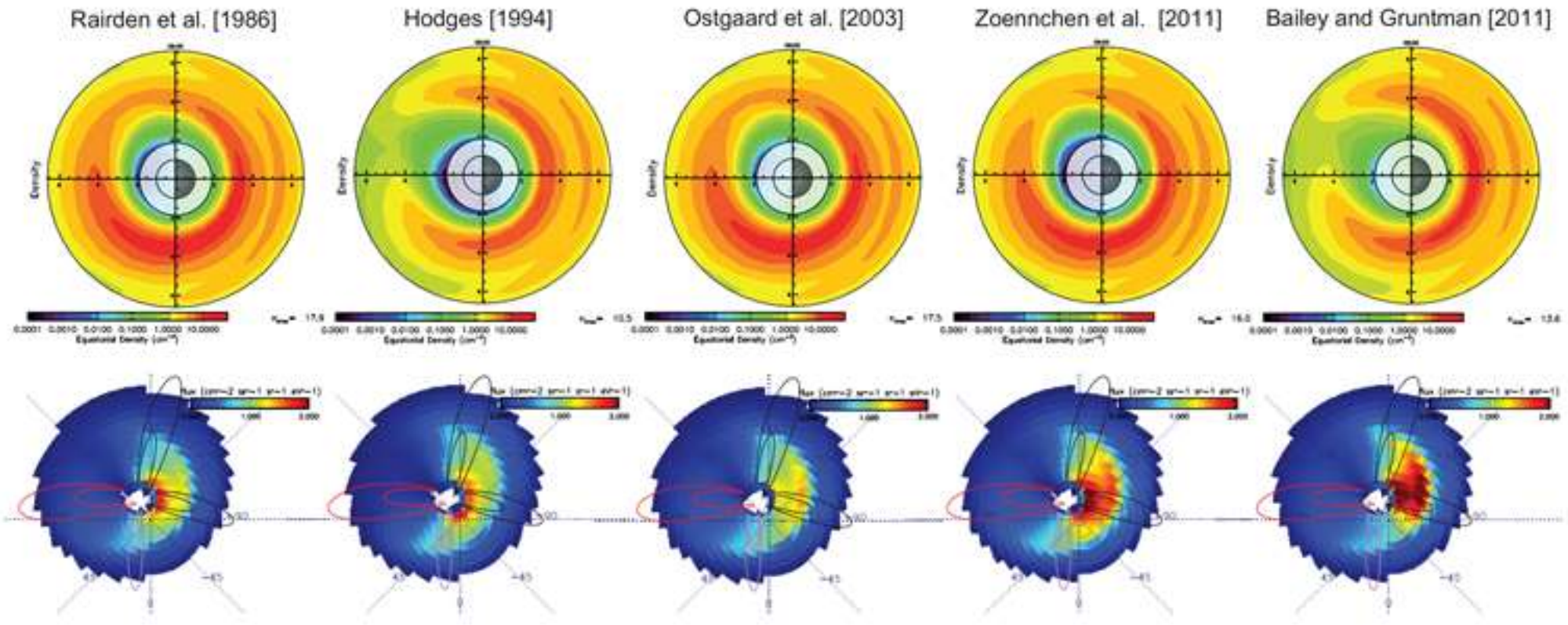


■ Loss of particles to the atmosphere due to the emptying of the loss cone (twice per bounce period τ_B) [Lyons, 1973]

$$\left\langle \left(\frac{\delta Q}{\delta t} \right)_{atm} \right\rangle = -\frac{Q}{\tau_{atm}} \quad \text{where} \quad \tau_{atm} = \begin{cases} \tau_B/2, & \text{inside the loss cone} \\ \infty, & \text{outside the loss cone} \end{cases}$$



Effects from Charge Exchange Loss



- (top) HEIDI simulated ion density in the equatorial plane for different neutral hydrogen distributions
- (bottom) HEIDI synthetic ENA images produced assuming these neutral hydrogen distributions

[Ilie et al., 2013]

RAM-SCB: Ring Current Loss Processes

■ Coulomb collisions with thermal plasma:

- Fokker-Planck equation considering energy degradation & pitch angle scattering

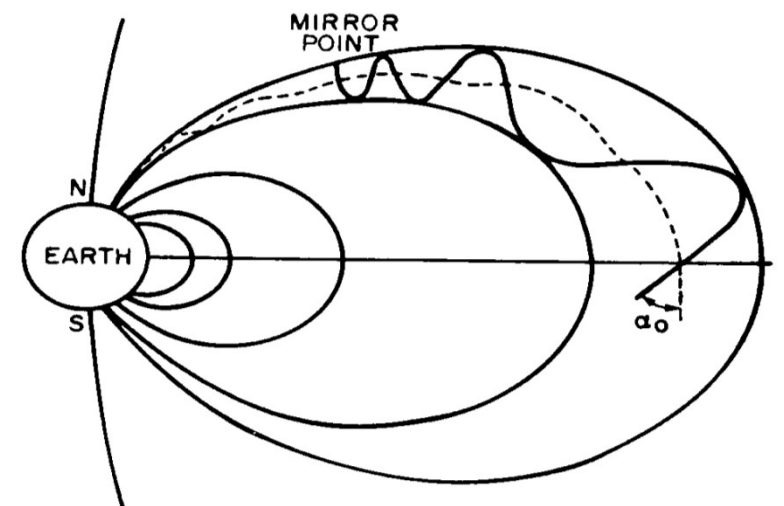
- plasmaspheric density model for e^- , H^+ He^+ , O^+ species [Rasmussen et al., 1993]

$$\left\langle \left(\frac{\delta Q}{\delta t} \right)_{cc} \right\rangle = \frac{1}{\sqrt{E}} \frac{\partial}{\partial E} \left\{ \sqrt{E} \left\langle \left(\frac{dE}{dt} \right)_{cc} \right\rangle Q \right\} + \frac{1}{h(\mu_o) \mu_o} \frac{\partial}{\partial \mu_o} \left[\langle D_{cc} \rangle h(\mu_o) \mu_o \frac{\partial Q}{\partial \mu_o} \right]$$

■ Plasma waves scattering: quasi-linear theory

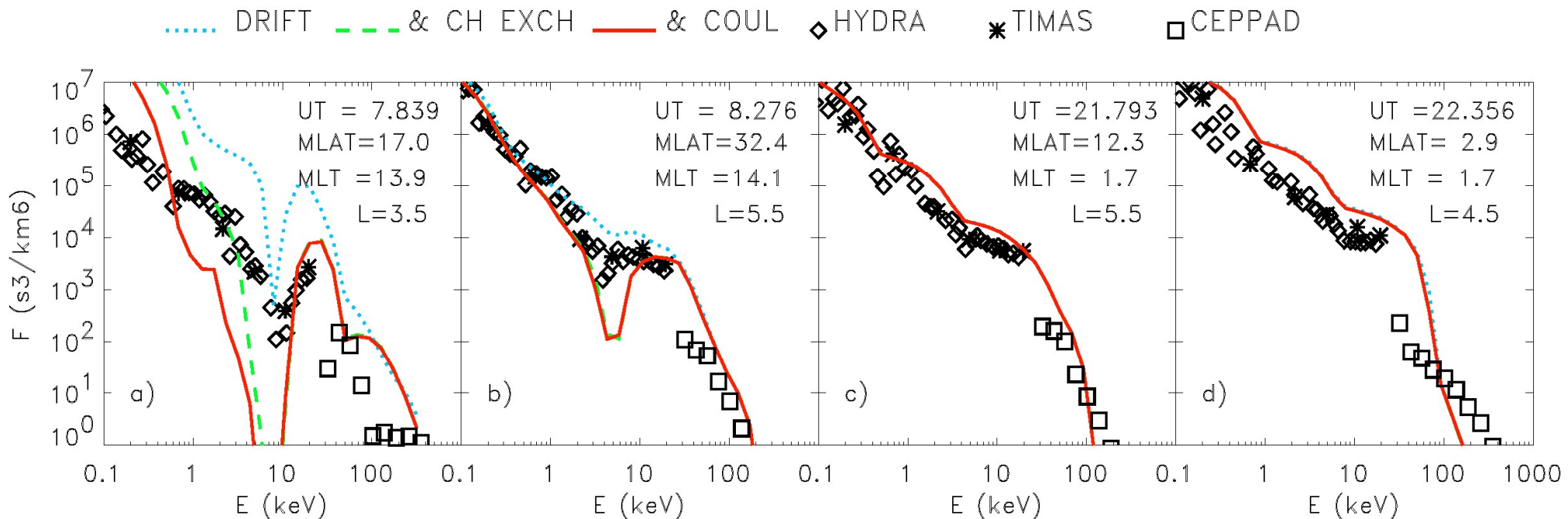
[Kennel and Engelmann, 1966; Lyons and Williams, 1984]

where $\langle D_{\mu_o \mu_o} \rangle$ are quasi-linear diffusion coefficients including heavy ion components [Jordanova et al., 1996]



Effects of Collisional Losses

Comparison of model results with POLAR data: March 1996



Larger effect on:

- postnoon spectra
- low L shells
- high magnetic latitudes
- slowly drifting \sim 1-30 keV ions

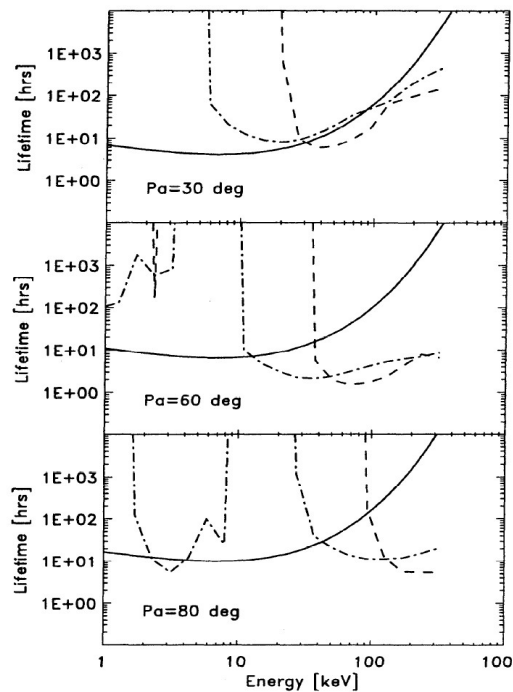
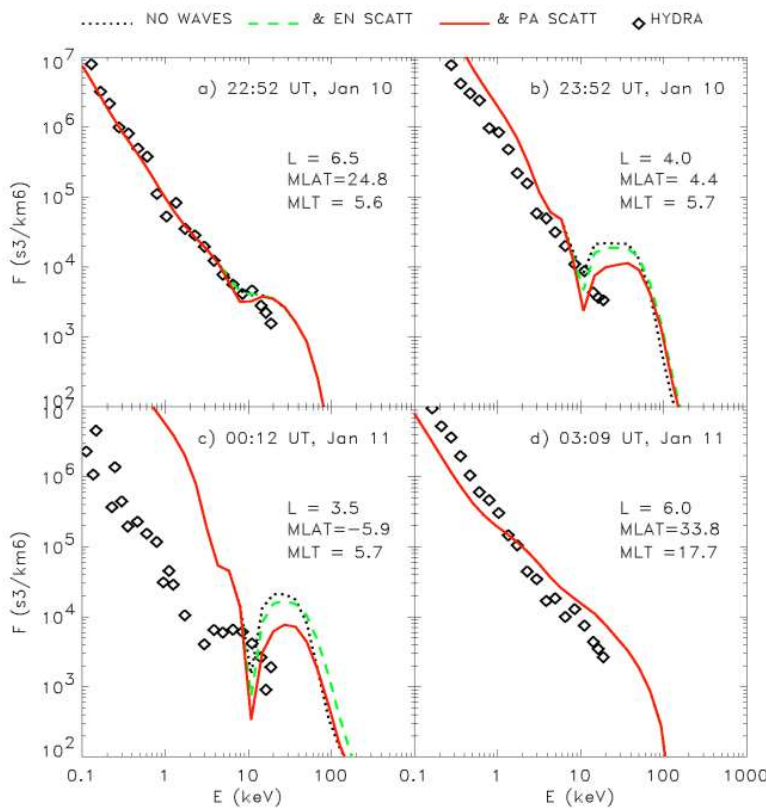
[Jordanova et al., 1999]

Effects of Wave-Particle Interactions

Lifetime of ring current **protons**

determined by:

- Charge exchange losses
- WPI in **electron-proton** plasma
- - - WPI in plasma consisting of
77% H⁺, 20% He⁺, and 3% O⁺



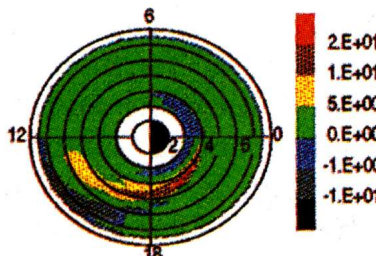
$$L=4$$

$$N_e = 500 \text{ cm}^{-3}$$

[Jordanova et al., 1996]

RAM results & Polar/HYDRA data comparison:

- **Pitch angle** scattering by EMIC waves has larger effect than **energy** diffusion
- **Non-local** effects of WPI due to transport



[Jordanova et al., 1998]

This presentation is being recorded

Towards a Self-Consistent Wave-Particle Interactions Model

- Obtain the convective growth rate from the plasma dispersion relation for EMIC waves:

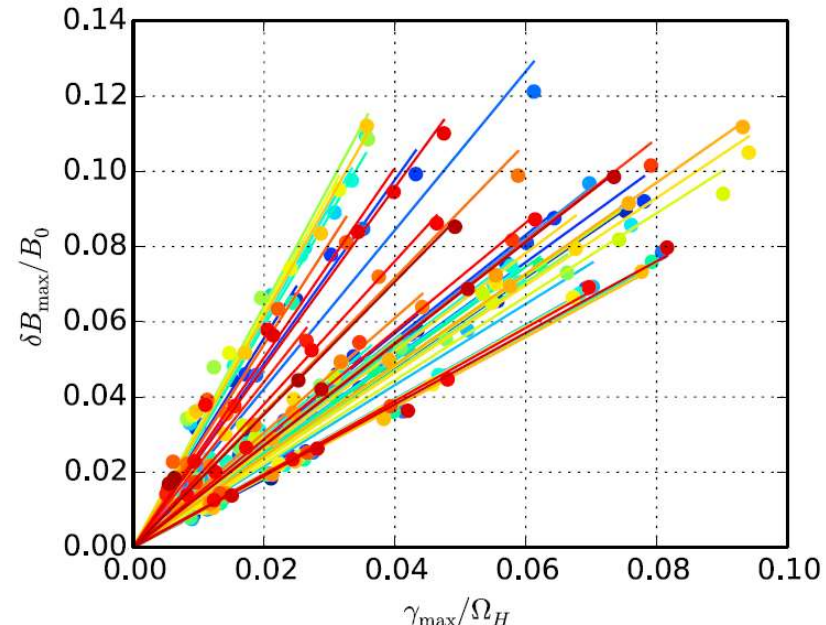
$$\frac{\gamma}{V_g} = \Psi(n_t, E_{II}, A_t)$$

where n_t , E_{II} , A_t are calculated with our kinetic model for H⁺, He⁺ and O⁺ ions

- Integrate the growth rates along wave paths to obtain the wave gain G (dB)
- Calculate the wave amplitude B_w using the semi-empirical relation:**

$$B_w = \begin{cases} B_{sat} = 10 \text{ nT} & \text{for } G > G_{max} \\ B_{sat} \times 10^{(G-G_{max})/G_{min}} & \text{for } G_{min} < G \leq G_{max} \\ < 0.1 \text{ nT (neglect)} & \text{for } G < G_{min} \end{cases}$$

[Jordanova et al., 2001; 2008]



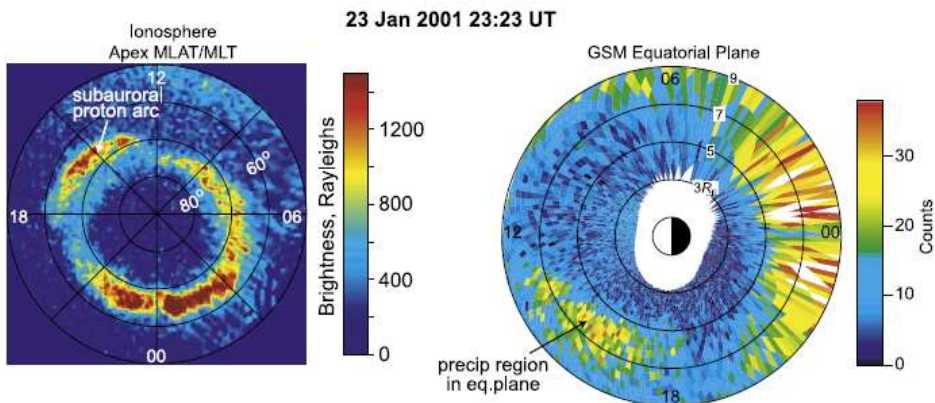
- Link the saturated EMIC wave amplitude $\delta B_{max}/B_0$ to plasma parameters using hybrid simulations [Bortnik et al., 2011]
- A new scaling fits most simulations using the linear growth rate of the most unstable mode:**
- The fitting parameter can be correlated with a function of these three plasma parameters:

$$\frac{\delta B_{max}}{B_0} = A \frac{\gamma_{max}}{\Omega_H}$$

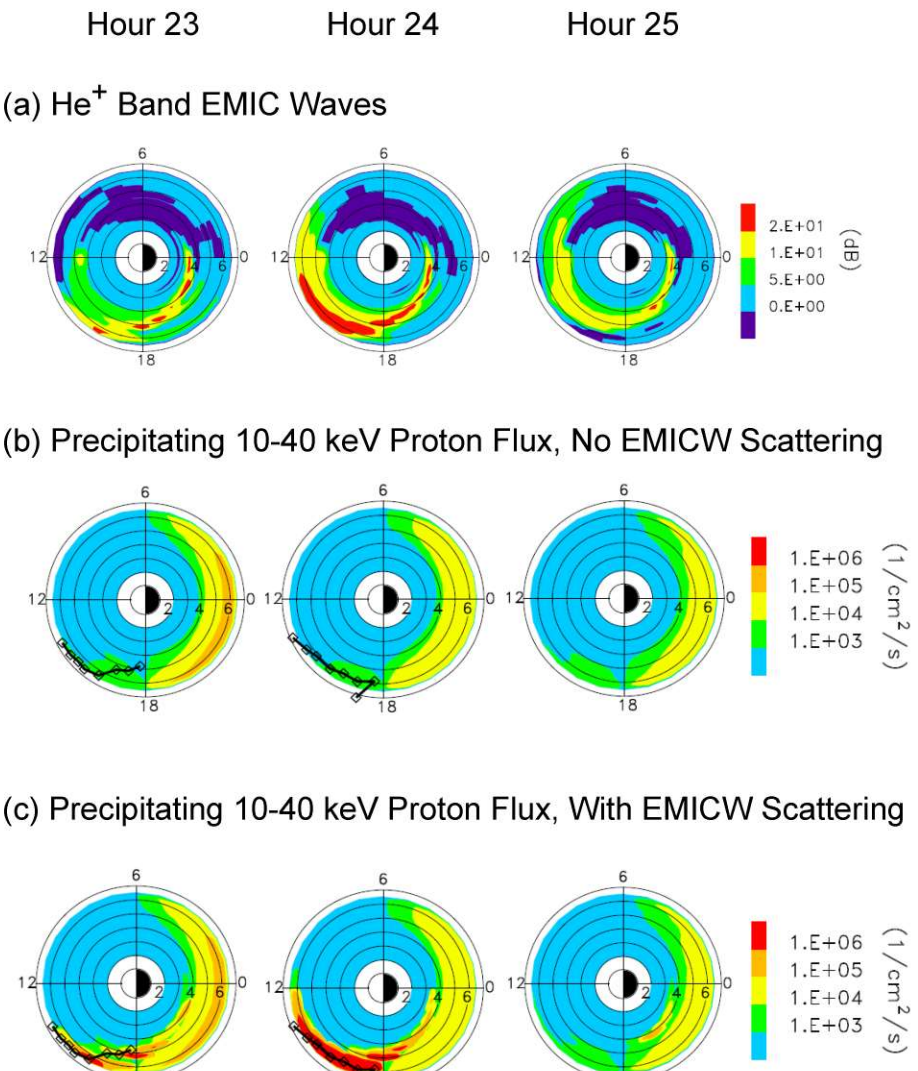
$$y = c_1 \sqrt{\tilde{\beta}_h} + c_2 \frac{n_h}{n_e} \tilde{\beta}_h + c_3 \tilde{\beta}_h \frac{n_{He}}{n_e} + c_4$$

[Fu et al., 2016]

Subauroral Proton Arcs: Observations and Modeling



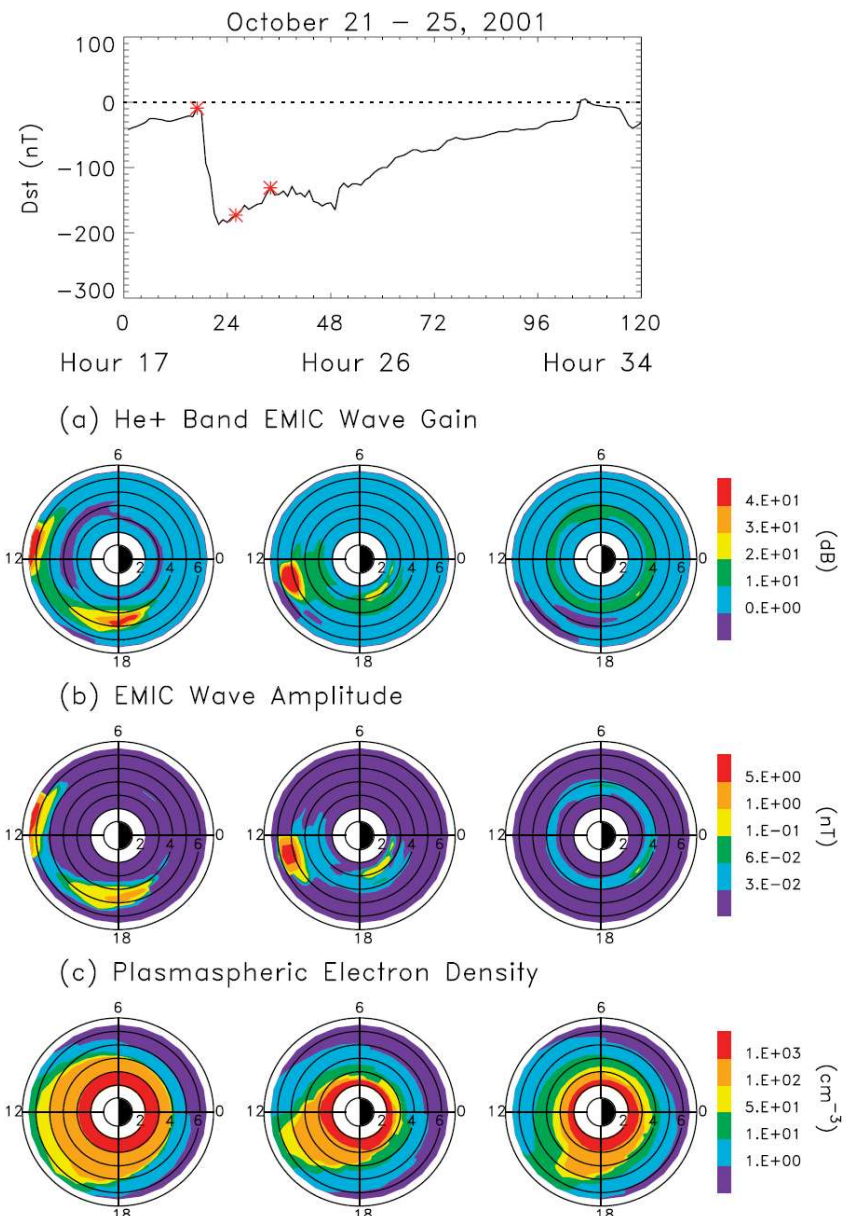
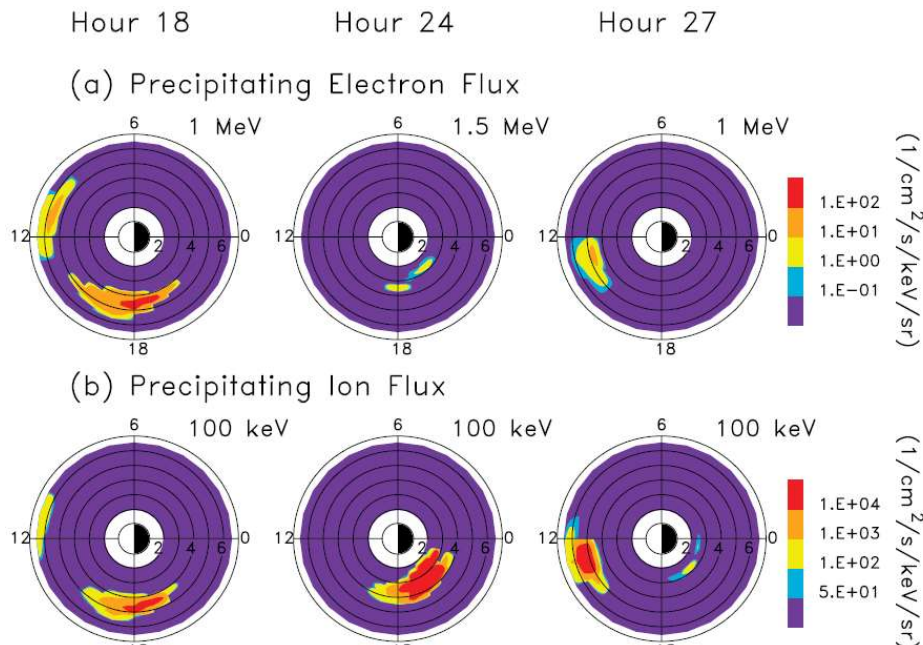
- Images from the **IMAGE/FUV** proton channel mapped to the GSM equatorial plane showing a detached subauroral proton arc on 23 Jan 2001
- Simulations with **RAM** indicating enhancement of **EMIC waves** within regions of spatial overlap of energetic ring current protons and high-density plasmaspheric plumes
- The location of the **proton precipitation** by EMIC waves matches very well the temporal and spatial evolution of FUV observations
⇒ cyclotron resonant wave-particle interactions are a viable mechanism for the generation of subauroral proton arcs



[Jordanova et al., 2007]

Effects on Radiation Belt Electron Precipitation

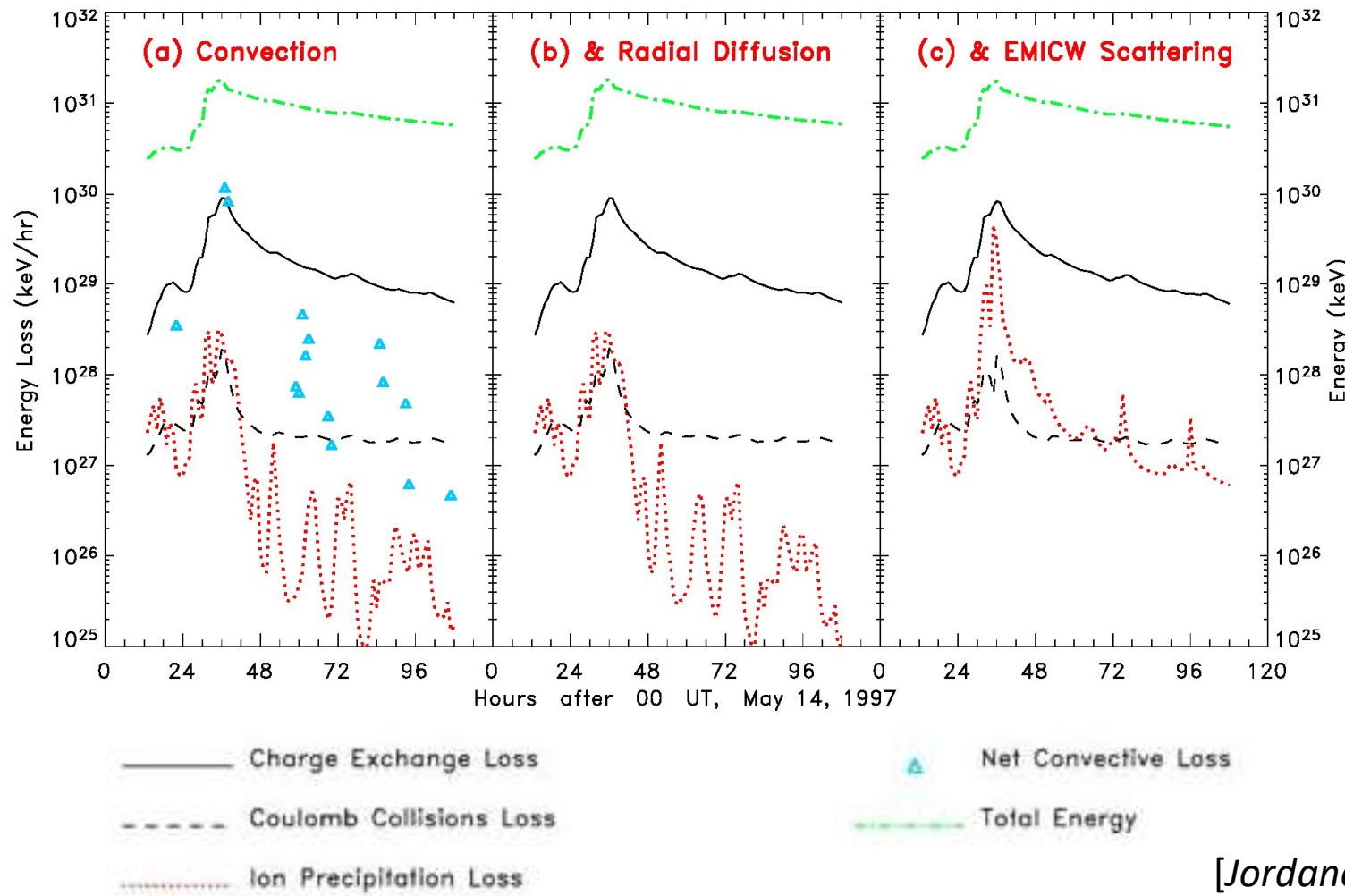
- Intense EMIC waves from the **He⁺ band** (between O⁺ and He⁺ gyrofrequency) are generated near **Dst minima** and are associated with the plasmapause or with plasmaspheric plumes
- Both **ion (keV)** and **electron (MeV)** **precipitation** is significantly enhanced within regions of EMIC wave instability by wave-particle interactions



[Jordanova et al., 2008]

This presentation is being recorded

Proton Ring Current Energy Losses

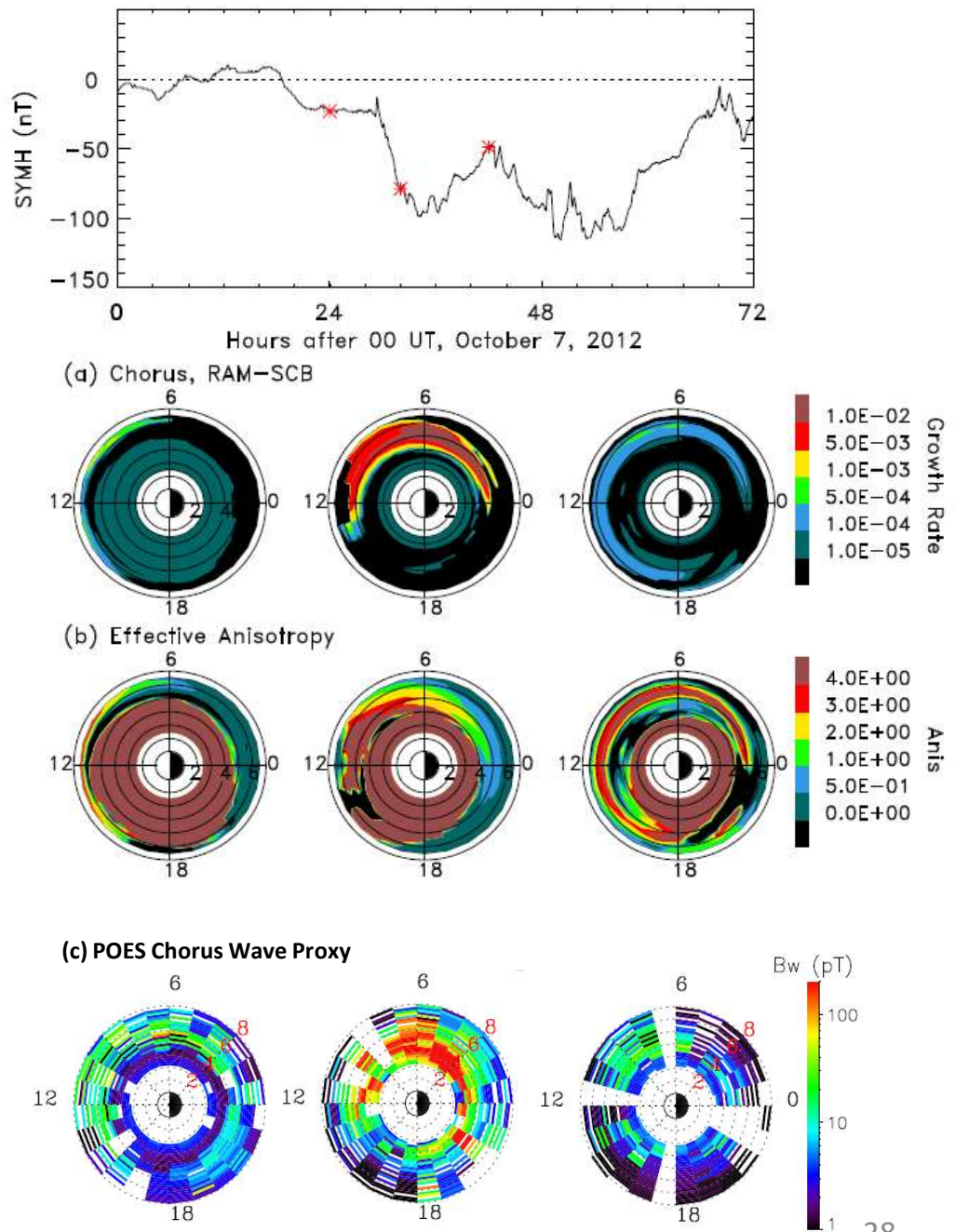


- Charge exchange is the dominant loss process
- The net **convective loss** and **ion precipitation from EMIC wave scattering** maximize near minimum Dst, reach the level of charge exchange loss

This presentation is being recorded

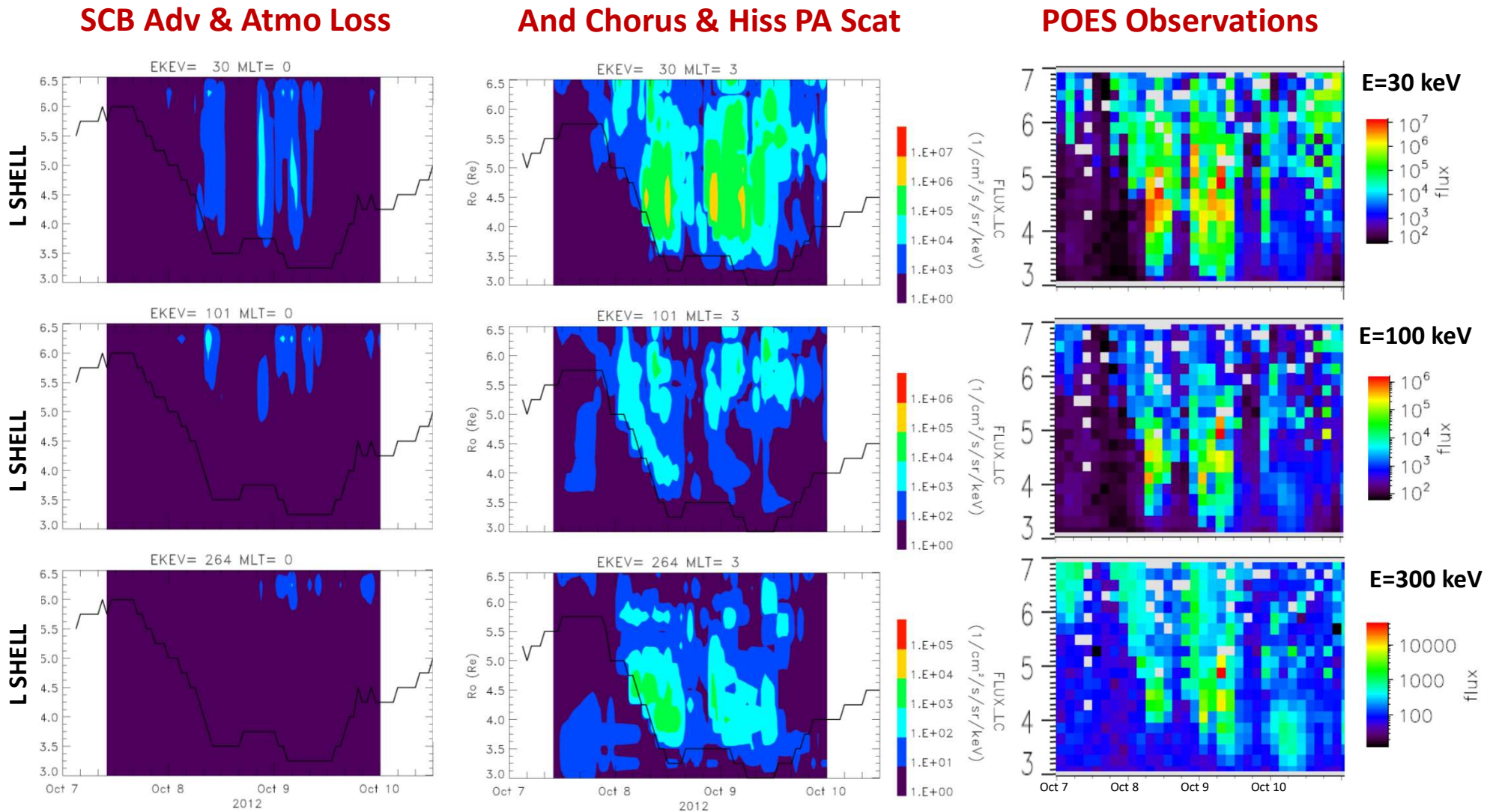
Global Chorus Wave Distributions

- Simulated with RAM-SCB chorus wave growth and anisotropy show significant increase due to electron transport and loss
- Global wave proxy derived from precipitating 30-100 keV electrons measured by the NOAA POES satellites during the storm [Chen *et al.*, 2014]
- Good agreement regarding the spatial and temporal evolution of the chorus wave instability during the storm main phase



This presentation is being recorded

RAM-SCB Simulations & NOAA Data: Precipitating Electron Flux



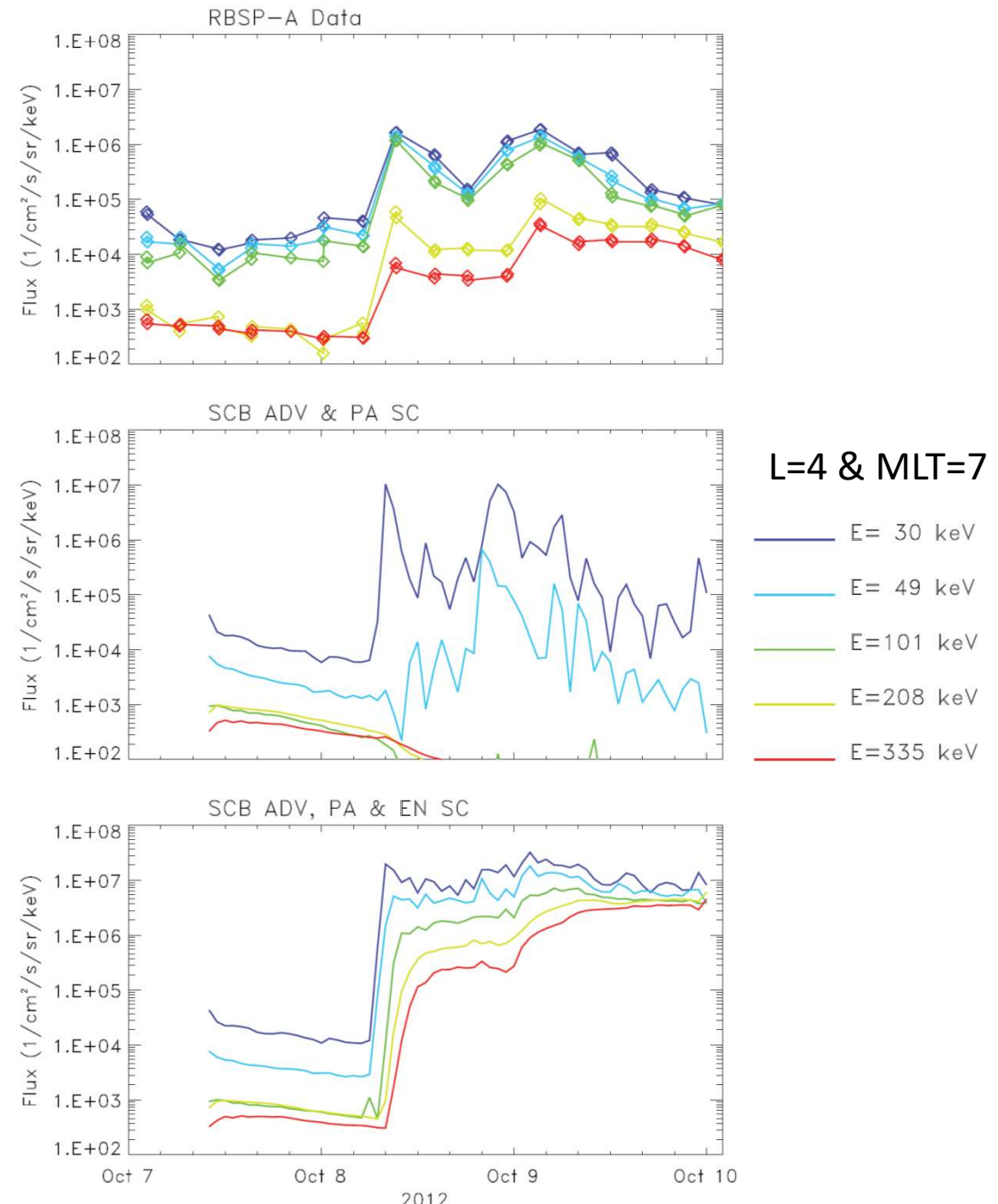
- RAM-SCB electron simulations as function of L and time (MLT=3)
- POES electron data (binned by three hours) in predawn (MLT 00-06) sector
- **Precipitating electron flux increases significantly in agreement with observations when plasma wave scattering is included**

This presentation is being recorded

RAM-SCB Results Compared with Van Allen Probes Data

- The simulated **electron flux increases due to transport** during the storm main phase at lower energies in agreement with observations
- The electron flux is significantly enhanced when **acceleration by chorus** is included
- RAM-SCB overestimates RBSP flux at high ($E > 100$ keV) energies by an order of magnitude during the first Dst min
=> Additional loss mechanisms or better temporal/spatial plasma wave distribution is needed to reproduce RBSP observations at high energies

[Jordanova et al., 2016]



This presentation is being recorded

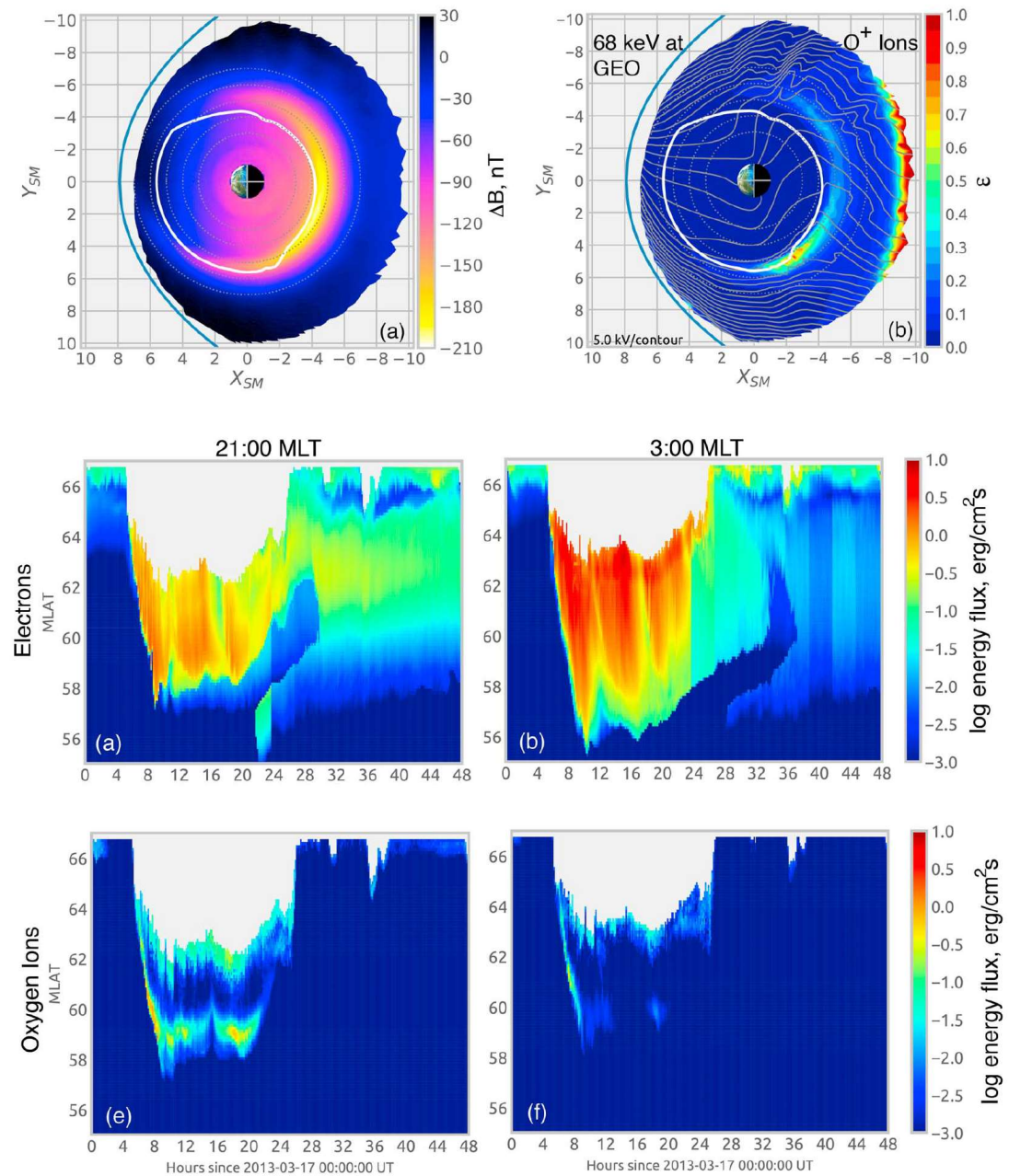
Effects from Field-Line Curvature Scattering

- Simulated equatorial magnetic field perturbation, equatorial epsilon parameter for O⁺ ions, and integrated precipitating energy flux over MLATs/time during 17 March 2013 storm with RCM-E [Chen *et al.*, 2019]

- **Sporadic and localized ion precipitation due to FLC scattering**

- The electron precipitation is more intense and reaches lower magnetic latitudes at early morning, where whistler wave activity is high during storm times

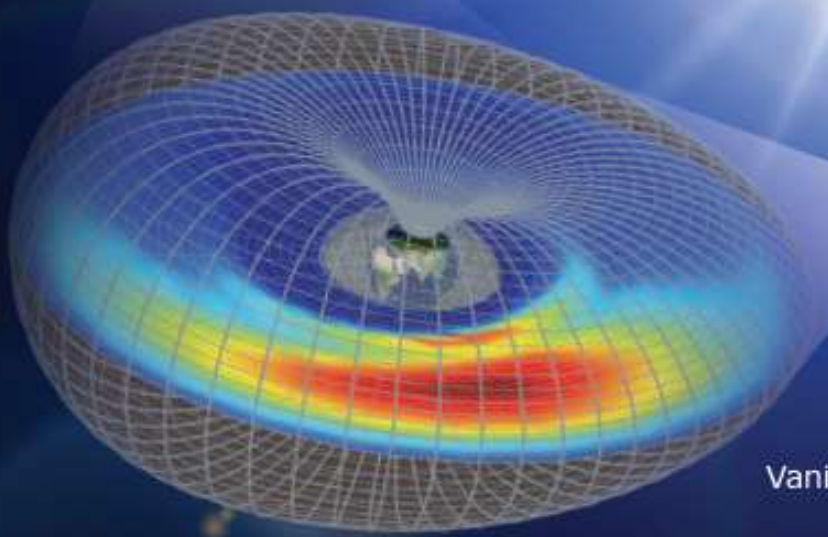
- A recent study using RAM-SCB [Yu *et al.*, 2020] found strong ion precipitation by FLC scattering at L>5 on the nightside, however comparisons with POES observations suggested that more ion precipitation is needed in the inner region



This presentation is being recorded

References

- Chen, M. W., et al. (2019). *J. Geophys. Res.*, 124, 4194–4216. <https://doi.org/10.1029/2019JA026545>.
- Daglis, I. A., et al. (1993). *Ann. Geophys.*, v. 11, pp. 685-696.
- Ebihara, Y., et al. (2004). *J. Geophys. Res.*, 109, A12209, doi:10.1029/2004JA010523.
- Engel, M., et al. (2019). *J. Geophys. Res.*, 124, 4233–4248, <https://doi.org/10.1029/2018JA026260>.
- Fok, M.-C., et al. (2001). *J. Geophys. Res.*, 106(A5), 8417–8424. <https://doi.org/10.1029/2000JA000235>.
- Fu, X., et al. (2016). *J. Geophys. Res. Space Physics*, 121, doi:10.1002/2016JA023303.
- Ganushkina, N. Y., et al. (2013) *J. Geophys. Res.*, 118, 82–98, doi:10.1029/2012JA017923.
- Hamilton, D. C., et al., 1988. *J. Geophys. Res.*, 93, 14,343, <https://doi.org/10.1029/JA093iA12p14343>.
- Ilie, R., et al. (2013). *J. Atmos. Sol. Terr. Phys.*, 99, 92–103, doi:10.1016/j.jastp.2012.03.010.
- Jordanova, V. K., (2006). *Geophys. Monogr. Ser.*, vol. 167, AGU, Washington, D. C., p. 77.
- Jordanova, V. K., et al. (1998). *Geophys. Res. Lett.*, 25(15), 2971–2974, <https://doi.org/10.1029/98GL00649>.
- Jordanova, V. K., et al. (2007). *J. Geophys. Res.*, 112, A08209, doi:10.1029/2006JA012215.
- Jordanova, V. K., et al. (2008). *J. Geophys. Res.*, 113(A3). <https://doi.org/10.1029/2008JA013239>.
- Jordanova, V. K., et al. (2010), *J. Geophys. Res.*, 115, A00J11, <https://doi.org/10.1029/2010JA015671>.
- Jordanova, V. K., et al. (2014). *Geophys. Res. Lett.*, 41, 2687–2694, doi: 10.1002/2014GL059533.
- Jordanova, V. K., et al. (2016). *J. Geophys. Res. Space Physics*, 121, doi:10.1002/2016JA022470.
- Liemohn, M. W., et al. (2004). *J. Geophys. Res.*, 109, A03209, doi:10.1029/2003JA010304.
- Lyons, L. R., and D. J. Williams, Quantitative Aspects of Magnetospheric Physics, D. Reidel, Dordrecht, 1984.
- Mouikis, C., et al. (2010). *J. Geophys. Res.*, 115, A00J16, doi:10.1029/2010JA015978.
- Rasmussen, C. E., et al. (1993). *Planet. Space Sci.*, v. 41, pp. 35-43.
- Tsyganenko, N. A., (1989). *Planet. Space Sci.*, v. 37, pp. 5-20.
- Wolf, R. A., et al. (1982). *J. Geophys. Res.*, 87(A8), 5949–5962. <https://doi.org/10.1029/JA087iA08p05949>.
- Yang, J., et al.(2015). *J. Geophys. Res.*, 120(9), 7416–7432. <https://doi.org/10.1002/2015JA021398>.
- Yang, J., et al. (2016). *Geophys. Res. Lett.*, 121(1), 374–379. <https://doi.org/10.1002/2015JA021901>.
- Young, D. T., et al., (1982). *J. Geophys. Res.*, 87, 9077, <https://doi.org/10.1029/JA087iA11p09077>.
- Yu, Y., et al. (2020). *J. Geophys. Res.*, 125, e2020JA027830, <https://doi.org/10.1029/2020JA027830>.
- Zaharia, S., et al. (2006). *J. Geophys. Res.*, 111, A11S14, <https://doi.org/10.1029/2006JA011619>.
- Zaharia, S., et al. (2008). *J. Atm. Sol.-Terr. Phys.*, 70(2), 511–518. <https://doi.org/10.1016/j.jastp.2007.08.067>.
- Zaharia, S., et al. (2010). *J. Geophys. Res.*, 115, A12228, <https://doi.org/10.1029/2010JA015915>.



Edited by

Vania K. Jordanova
Raluca Ilie
Margaret W. Chen

Ring Current Investigations

The Quest for Space Weather Prediction



- Ring Current Investigations: The Quest for Space Weather Prediction, Elsevier Book, 2020, <https://www.sciencedirect.com/book/9780128155714/ring-current-investigations?via=ihub=>
- Provides a detailed review of historical and recent advances in observations, theory and simulations of the Earth's ring current as part of the coupled magnetosphere-ionosphere system
- Compares the physics of ring currents at other strongly magnetized planets in the solar system, Jupiter, Saturn, Uranus and Neptune, with the ring current system at Earth
- Available for libraries in a "DRM-free" version (free PDF download for institution members)

Open Questions

- What determines where and when hot plasma is injected into the inner magnetosphere and what is the depth of particle penetration?
- How are the injected particles transported, what is the role of convective versus inductive electric fields?
- What are the effects of ion composition variability with geomagnetic and solar activity on ring current dynamics?
- What waves do the injected particles excite and how do these waves feed back on the acceleration and loss of the particles?
- What is the role of the ionosphere in sustaining the ring current?
- ...



This presentation is being recorded